Precipitation of dolomite from seawater on a Carnian coastal plain (Dolomites, northern Italy): evidence from carbonate petrography and Sr-isotopes

Maximilian Rieder[1], Wencke Wegner[2], Monika Horschinegg[2], Stephanie Klackl[1], Nereo Preto[3], Anna Breda[3], Susanne Gier[1], Urs Klötzli[2], Stefano M. Bernasconi[4], Gernot Arp[5], Patrick Meister[1]

[1] Department of Geodynamics and Sedimentology, University of Vienna, Althanstr. 14, 1090 Vienna, Austria

[2] Department of Lithospheric Research, University of Vienna, Althanstr. 14, 1090 Vienna, Austria

[3] Department of Geosciences, University of Padova, Via Gradenigo 6, 35131 Padova, Italy

[4] Geological Institute, ETH Zürich, Sonneggstr. 5, 8092 Zürich, Switzerland

[5] Geoscience Centre, University of Göttingen, Goldschmidtstr. 3, 37077 Göttingen, Germany

Correspondence: Patrick Meister (patrick.meister@univie.ac.at)

Abstract. The geochemical conditions conducive to dolomite formation in shallow evaporitic environments along the Triassic Tethyan margin are still poorly understood. Most of the Triassic dolomites in the Austroalpine and the South Alpine realm are affected by late diagenetic or hydrothermal overprinting, but recent studies from the Carnian Travenanzes Formation (South Alpine) provide evidence of primary dolomite. Here a petrographic and geochemical study of ~~the~~ dolomites intercalated in a 100-m-thick Carnian sequence of distal alluvial plain deposits is presented to gain better insight into the conditions and processes of dolomite formation. The dolomites occur as 10- to 50-cm-thick homogenous beds, mm-scale laminated beds and nodules associated with palaeosols. The dolomite is nearly stoichiometric with slightly attenuated c-reflections. Sedimentary structures indicate that the initial primary dolomite or precursor phase consisted largely of unlithified mud. Strontium isotope ratios ($^{87}Sr/^{86}Sr$) of homogeneous and laminated dolomites reflect Triassic seawater, suggesting precipitation in evaporating seawater in a coastal ephemeral lake or sabkha system. However, the setting differed from modern sabkha or coastal ephemeral lake systems by seasonally wet conditions with ~~a~~ significant siliciclatic input and inhibition of significant lateral groundwater

flow ~~through~~ impermeable clay deposits, thus represent~~ing~~ a non-actualistic system in which dolomite formed ~~along the ancient Tethyan margin~~.

Keywords Dolomite, Sr-isotopes, sabkha, alluvial plain, peritidal platform, Travenanzes Formation, ephemeral lake, authigenic carbonate.

1 Introduction

The formation of dolomite [$CaMg(CO_3)_2$] under Earth surface conditions in modern and ancient environments is still a major unsolved problem in sedimentary geology. Dolomite does not precipitate from modern open ocean water, apparently~~,~~ because its nucleation and growth is inhibited by a high kinetic barrier. For the same reason ~~its~~ precipitation under laboratory conditions has been difficult (cf. Land, 1998), and therefore the factors that may have influenced dolomite formation through Earth ~~history, giving rise to a significant part of the sedimentary record,~~ also remain poorly constrained. Van Tuyl (1916) discussed several competing theories, one of which was the chemical theory, where dolomite is a primary precipitate, ~~hence,~~ forming as ~~a~~ result of ~~the conditions~~ prevailing in the depositional environment. In contrast, stable isotope and fluid inclusion data often indicate that massive dolomites formed due to replacement of precursor calcium carbonate during burial diagenesis, i.e., at higher temperature and under conditions decoupled from the ancient depositional environment. Chilingar (1965) suggested that the portion of dolomite in carbonates increases with geological age, implying ~~a~~ replacement during burial. However, burial dolomitization requires a mechanism pump~~ing~~ large volumes of Mg-rich water through porous rock (Machel, 2004) and is not always a viable process. There is evidence that ~~at certain times in Earth's history,~~ large amounts of dolomite could have formed under near-surface conditions (penecontemporaneous dolomite), and several studies linked the abundance of dolomite to

secular variations in seawater chemistry, with ~~preferred~~ dolomite ~~formation~~ during times of "calcite seas" (Given and Wilkinson, 1987; Warren, 2000; Burns et al., 2000).

In the Tethyan realm, penecontemporaneous dolomite formation seems to have prevailed during the Triassic (Meister et al., 2013, and references therein), in an "aragonite sea", while elsewhere dolomite was not particularly abundant (cf. Given and Wilkinson, 1987). In Norian shallow water dolomites of the Dolomia Principale, Iannace and Frisia (1994) measured oxygen isotope values as positive as +3.5‰, suggesting ~~a~~ formation at Earth surface temperatures, whereas dolomites ~~of~~ the overlying ~~early~~ Jurassic units typically show signatures of burial diagenetic overprint. Frisia et al. (1994) interpreted these dolomites to be an early diagenetic replacement of precursor carbonate. In a recent study, Preto et al. (2015) suggested that the dolomites of the Carnian Travenanzes Formation (Fm.) in the Venetian Alps are primary precipitates, i.e. they precipitated directly from ~~a~~ solution in the sedimentary environment and not by replacement of a precursor phase during burial. This interpretation is based on high-resolution transmission electron microscope (HR-TEM) analysis showing nanometre-sized crystal aggregates within single micron-scale dolomite crystals. The nano-crystal structures were not replaced by any of the dolomite phases described by Frisia and Wenk (1993) in Late Triassic dolomites of the Southern Alps~~, and~~ they ~~show similarity~~ to dislocation-ridden Mg-rich phases observed in modern sabkha ~~dolomite~~ and interpreted as primary (Frisia and Wenk, 1993). This finding is intriguing, not only because it is consistent with primary dolomite formation ~~already discussed~~ by Van Tuyl (1916) and observed in many modern environments (e.g., Sabkha of Abu Dhabi: Illing, 1965; Wenk et al., 1993; unlithified dolomite is also mentioned in Bontognali et al., 2010; and Court et al., 2017; Deep Springs Lake, California: Jones, 1965; Clayton et al., 1968; Meister et al., 2011; Coorong Lakes: Von der Borch, 1976, Rosen et al., 1989, Warren et al., 1990; Brejo do Espinho, Brazil; Sánchez-Román et al., 2009; Lake Acigöl, Turkey: Balci et al., 2016; Lake Neusiedl, Austria: Neuhuber et al., 2015; Lake Van: McCormack et al., 2018), but it also provides a window into

ancient primary dolomite formation pathways. This finding is also consistent with recent experiments by Rodriguez-Blanco et al. (2015), demonstrating a nano-crystalline pathway of dolomite nucleation and growth. Critically, nanometre size nuclei show a different surface energy landscape compared to macroscopic crystals, allowing for potentially lower energy barriers, perhaps modified by organic matter, microbial effects, clay minerals or particular water chemistry, and thus, promoting ~~a~~ spontaneous precipitation of dolomite.

The interpretation of primary dolomite in the Travenanzes Fm. needs further validation by nano- and atomic scale analyses and further petrographic and geochemical investigations to establish the environmental and geochemical conditions on this Carnian platform. In particular, the origin of ionic solutions conducive to dolomite formation is still unclear. Comparison with modern environments shows that ionic solutions may either be seawater-derived, as shown for the sabkhas along the Persian Gulf coast, where several hydrological mechanisms were discussed (Adams and Rhodes, 1960; Hsü and Siegenthaler, 1969; McKenzie et al., 1980, McKenzie, 1981; see Machel, 2004, for an overview; cf. also Teal et al., 2000), or derived from continental groundwater, as shown for the coastal ephemeral lakes of the Coorong area (Australia; Alderman and Skinner, 1957; Von der Borch et al., 1976, Rosen et al., 1989; Warren et al., 1990). While both types of fluid become concentrated during evaporation and, perhaps, modified by the precipitation of carbonates and evaporites, ~~giving rise to abundant dolomite formation,~~ it remains unclear which mechanism prevailed on the Carnian platform.

The Travenanzes Fm. differs from ~~these potential~~ modern analogues in ~~its~~ large amounts of clay. ~~In fact,~~ dolomites occur in the Travenanzes Fm. as ~~beds~~ intercalated in a 100-m-thick sequence of red clay, deposited on a distal alluvial plain, presumably under seasonally wet conditions. This facies shows, except for the horizons containing marine fossils, striking similarity to ~~a~~ Germanic Keuper facies, which represents an extended and entirely continental playa lake system, also ~~showing~~ intercalations of primary dolomite in red clay (Reinhardt and

Ricken, 2000). Although the Travenanzes Fm. is clearly located, palaeogeographically, in the Tethyan depositional region (Breda and Preto, 2011), its facies separation from a Germanic Keuper facies may not be precisely coincident with palaeogeographic features, such as the Vindelician high zone. We suggest that the composition and origin of ionic solutions conducive to primary dolomite formation, either ~~from~~ continental water or seawater, is also an indicat~~or for the~~ palaeogeographic separation between the two facies zones.

Here we provide a detailed investigation of dolomites of the Travenanzes Fm. to reconstruct the processes and factors conducive to dolomite formation. We specifically searched for sedimentary structures indicating that the initiall~~y deposited~~ authigenic carbonate was ~~still~~ unlithified, as ~~it~~ would be expected if it spontaneously precipitated from the shallow water bodies of ephemeral lakes or tidal ponds. Radiogenic Sr isotope ratios ($^{87}Sr/^{86}Sr$) were measured in the dolomites and compared with the ~~known~~ Triassic seawater Sr-isotope curve (Veizer et al., 1999; McArthur et al., 2012) to determine if ~~the~~ ionic solutions conducive to dolomite formation ~~are~~ derived from seawater or from continental runoff. Values were also compared to dolomites from modern environments and to dolomites of clear continental origin from the Germanic Keuper. Based on ~~the~~ new insights we discuss possible scenarios of dolomite formation that could have prevailed along the ~~Triassic~~ western Tethys margin~~s~~ and in similar evaporative environments.

2 Geological setting

The Dolomite mountains (Southern Tyrol and Venetian Alps; Fig. 1a) are well known for their characteristic peaks consisting of Triassic carbonate platform limestones and dolomites. These platforms developed all along the margins of the western Tethys ocean (Stampfli and Borel, 2002), and are separated by deep basins in the middle Triassic and form an extended coastal plain during the Carnian and Norian. The Adriatic plate rotated ~~by~~ almost 90° counter clockwise ~~during~~ alpine orogeny (Ratschbacher et al., 1991; Handy et al., 2010). As a result,

the deep-water environments are found to the north in today's tectonic position although they were originally located to the east (Fig. 1a). In the Dolomites, the Triassic paleogeography was largely preserved in spite of Alpine deformation because the Dolomites form a ca. 60 km wide pop-up structure bound by the periadriatic line to the north and northwest and the Valsugana fault to the southeast (Fig. 1a, inset). Therefore, the Dolomites were never buried to greater depth and have not experienced a metamorphic overprint (Doglioni, 1987). The colour alteration index of conodonts in the Heiligkreuz Fm., underlying the Travenanzes Fm. in this region, is 1, suggesting maximum burial temperatures of less than 50°C which are confirmed by biomarker data (Dal Corso et al., 2012).

The Travenanzes Fm. lies unconformably above the Heiligkreuz Fm., and is overlain by the Dolomia Principale (Hauptdolomit) with a transgressive boundary (Fig. 1b). Presumably as a result of a change in climate and increasing humid episodes during the Carnian, large amounts of siliciclastic material were deposited, entirely filling the more than 100 m deep basins between the carbonate platforms of the Cassian dolomite (Gattolin et al., 2013; 2015). These basin-filling deposits form a coastal succession or mixed carbonate-siliciclastic ramp, including large clinoforms with sandstones and conglomerates (Heiligkreuz Fm.; see Preto and Hinnov, 2003; Gattolin et al., 2013; 2015). The overlying Travenanzes Fm. was deposited on an extremely flat topography, as it consists of ca. 100-m-thick red and green claystone with intercalated dolomites, evaporites and siliciclastic beds (Fig. 2; Kraus, 1969; Breda and Preto, 2011). In a south-north transect, it shows a typical interfingering between alluvial deposits with conglomerates and sandstones to the south and a carbonate-dominated peritidal to sabkha facies to the north (Breda and Preto, 2011). The upper boundary to the Dolomia Principale is time-transgressive, i.e., it becomes younger from north to south. The Travenanzes Fm. consists of three transgressive-regressive cycles, with the highstand deposits showing identical peritidal carbonate facies as the Dolomia Principale (Breda and Preto, 2011). The

boundary ~~to~~ the Dolomia Principale is defined by the last occurrence of siliciclastic material (Gianolla et al., 1998).

The depositional environment of the siliciclastic facies ~~in~~ the Travenanzes Fm. has been interpreted as a dryland-river system by Breda and Preto (2011). Such a system occurs in arid environments if rivers drain into a coastal alluvial plain, but do not reach the coast. Evaporation along the way may lead to the formation of playa lakes~~, whereas~~ on the seaward side extended evaporative tidal areas, i.e., sabkhas, develop. Both types of environment are well known for giving rise to modern dolomite formation (see references above). As the Southern Alps were located in tropical latitudes, a warm arid climate, perhaps influenced by a monsoon ~~effect, had~~ developed (Muttoni et al., 2003). Rivers provided large amounts of clay, ~~becoming~~ partially oxidized under subaerial conditions, a typical red and green clay succession containing palaeosols ~~developed~~.

This facies is widespread throughout the Alpine and Tethyan realm during the Carnian, but ~~the same~~ deposits are strongly deformed by alpine tectonics in most Austroalpine units, forming a characteristic band of rauhwacke, the "Raibl beds" (e.g., Czurda and Nicklas, 1970). In the Travenanzes Fm. the entire sequence ~~still shows~~ its depositional architecture, providing a pristine archive to study the ~~diverse~~ intercalated dolomites.

The Carnian and Norian deposits of the Keuper in the endorheic Germanic Basin ~~show a~~ similar facies as the Travenanzes Formation. The Germanic deposits are described in more detail by Reinhardt and Ricken (2000; and references therein), and they clearly represent continental playa lake deposits. Here they are only included for comparison with the Travenanzes Formation.

3 Methods

3.1 Petrographic and mineralogical analysis

182 A total of 39 hand specimens were collected from the stratigraphic section at Rifugio
183 Dibona 5 km west of Cortina d'Ampezzo (46.532727N/12.067161E; Fig. 1; Breda and Preto,
184 2011). Additional samples of Triassic dolomites from the Germanic Basin (Weser Fm. and
185 Arnstadt Fm. near Göttingen, Northern Germany) and modern dolomite from the Coorong
186 Lagoon (South Australia) and Deep Springs Lake (California) were also analysed for
187 comparison. Polished thin sections were carbon coated for analysis under the scanning
188 electron microscope (SEM) using a FEI Inspect S-50 SEM (Thermo Fisher Scientific,
189 Bremen, Germany). Element contents were determined semi-quantitatively using an EDX
190 detector (EDAX Ametek, New Jersey, United States) under high vacuum, a spot size 5.0 and
191 12.5 kV beam voltage at a working distance of 10 mm. Differences in mineralogy at the
192 micron scale were mapped in backscatter mode with high contrast.

193 For bulk mineralogical analysis three dolomite samples were milled with a disk mill. Clay
194 mineralogy was determined on 40 g aliquots that were leached two times for 24 h in 250 ml of
195 25% acetic acid to dissolve all carbonate (Hill and Evans, 1965). The clay mineral separates
196 were washed three times with H_2O and centrifuged. The grain size fraction <2 µm was
197 collected by sedimentation in an Atterberg cylinder after 24 h 33 min. Oriented samples were
198 prepared by pipetting the suspensions (10 mg clay/ml) on glass slides and analysed after air
199 drying. To identify expandable clay minerals, the samples were additionally saturated with
200 ethylene-glycol and heated to 550°C (Moore and Reynolds, 1997). X-ray diffraction analysis
201 of bulk samples and clay mineral separates was performed with a PANalytical X'Pert Pro
202 diffractometer using CuKα radiation with 40 kV and 40 mA. The samples were scanned from
203 1.76° to 70° 2ϑ with a step size of 0.0167° and 5 s per step. The X-ray diffraction patterns
204 were interpreted using the Panalytical software "X'Pert High score plus" and Moore and
205 Reynolds (1997) for the clay minerals.

206 Total organic carbon (TOC) and total inorganic carbon (TIC) contents were determined for
207 seven samples of pure claystone, not containing any dolomite layers or nodules. This material

208 was used as carbonate-free control for acid leaching experiments as explained below. Ca. 0.2
209 g of dry sample powder was measured in a LECO RC-612 multiphase carbon analyser, at the
210 Department of Environmental Geosciences at the University of Vienna, with a temperature
211 ramp of 70°C per min to a maximum temperature of 1000°C.
212
213 **3.2 Carbon and oxygen isotope analysis**
214 Carbon and oxygen isotopes were measured on 28 samples which where micro-drilled
215 from thin section cuttings (see below). The samples were analysed with a Delta V Plus mass
216 spectrometer coupled to a GasBench II (Thermo Fisher Scientific, Bremen, Germany) at ~~the~~
217 ETH Zürich (Zürich, Switzerland) following the procedure described in Breitenbach and
218 Bernasconi (2011). The precision was better than 0.1‰ for both isotopes. The oxygen isotope
219 values were corrected for kinetic fractionation during dissolution of dolomite in anhydrous
220 phosphoric acid at 70°C, using a fractionation factor of 1.009926 (Rosenbaum and Sheppard,
221 1986).
222
223 **3.3 Element analysis**
224 Total element concentrations were measured in leachates of the same three dolomite
225 specimen analysed by XRD and two claystones with the lowest inorganic carbon content. The
226 purpose of these measurements was to test the efficiency of the sequential extraction
227 procedure used for Sr-isotope analysis, and to determine potential origins of the Sr. The
228 samples were homogenized in an agate pestle and mortar and 100 mg of the homogenized
229 powder ~~were~~ weighed into centrifuge tubes. The samples were reacted ~~in~~ 10 ml 0.1 N acetic
230 acid and placed on a shaker for two days. The sample ~~was~~ centrifuged and the supernatant
231 was stored separately. The leaching step was repeated with 10 ml of 1 N acetic acid. Five ml
232 of each fraction ~~were~~ used for element concentration analysis (the rest was further processed
233 for Sr-isotope analysis; see below). The solutions were evaporated on a heating plate and the

residues were redissolved in 5 ml 2.5 N HNO_3. This step was repeated with 5 ml 5% HNO_3. Concentrations were measured with a Perkin Elmer 5300 DV ICP-OES at the Department for Environmental Geosciences (University of Vienna). Detection limits for the different elements in rock (µmol/g) were: Al: 0.185, Ca: 0.025, Fe: 0.090, K: 0.026, Mg: 0.041, Mn: 0.002, Na: 0.004, P: 0.032, Ti: 0.002, Ba: 0.001, Sr: 0.001 and Rb: 0.012. The precision of the measurements (relative standard deviation; RSD) for ~~the elements~~ Al, Ca, K, Mg, Ti, Ba and Sr was ≤0.9% and for ~~the elements~~ Fe, Mn, Na, Rb, P ~~it~~ was ≤6.8%.

3.4 Radiogenic Sr-isotope analysis

To ensure that Sr from the pure dolomite phase is extracted, specific areas free of clay minerals were ~~recognized~~ by SEM and identified using an Olympus SZ61 microscope equipped with a MicroMill sampling system (Electro Scientific Industries). Eleven samples were drilled over ~~a square~~ area of 5-10 mm^2, or along a line in laminated rocks, to a depth of 350 µm. To prevent the powder from being ~~blown away,~~ the samples were drilled within a drop of MilliQ-H_2O, and the suspension was transferred to a centrifuge tube using a pipette. ~~Also,~~ bulk samples, clay samples, pure celestine and barite purchased from W. Niemetz (Servitengasse 12, 1090 Vienna, Austria), pure dolomite powder from Alfa Aesar (Thermo Fisher – Kandel – GmbH, Postfach 11 07 65, 76057 Karlsruhe, Germany) and a fragment of a single dolomite crystal were analysed as controls. They were crushed to a powder in an agate mortar and pestle. Dolomite, barite, and celestine were mixed in a similar ratio as they occur in the dolomites of the Travenanzes Fm. and run through the entire procedure as a control of extraction efficiency. 14 mg of rock powder was weighed out for isotope analysis.

~~As additional precaution to extract the most pure dolomite phase for Sr-isotope analysis, a~~ sequential extraction was used. The extractions were routinely performed in 2 ml or 15 ml polypropylene tubes ~~with cap~~ at room temperature on a shaker for 10 min to 24 h. The following leaching reagents (always 2 ml) were used: 1 M NaCl, 3.3 M KCl, 0.1 N acetic

acid, 1 N acetic acid and 6 N HCl. Each reaction step was repeated once, and the residues were washed with 2 ml of MilliQ H_2O after each step to remove remains of the previous solvent.

Sr was separated from interfering ions (e.g. Fe, K, Rb and Ca) using an ion exchange column packed with BIO RAD AG 50W-X8 resin (200-400 mesh, hydrogen form). Leachates were evaporated, dissolved in 6 N HCl and 2.5 N HCl and loaded to the column in 2 ml 2.5 N HCl. ~~Then~~ 51 ml of 2.5 N HCl were run through the column to wash out the interfering ions. ~~The~~ Sr was eluted with a further 7 ml 2.5 N HCl and dried after collection. Total procedural blanks for Sr were <1 ng and were taken as negligible (the amounts of strontium in the samples were always higher than 100 ng).

The isotopic composition of Sr was measured with a Triton (Thermo Finnigan) thermal ionisation mass spectrometer. Sr fractions were loaded (dissolved in 1 µl H_2O) as chlorides and vaporized from a Re double filament. The double filament configuration was used to accelerate detachment of ~~the~~ Sr from the filament. The cup configuration was calibrated such that masses 84, 85 (centre cup), 86, 87 and 88 are detected. The NBS987 Sr isotope standard (number of replicates = 40) shows a $^{87}Sr/^{86}Sr$-ratio of 0.710272 ±0.000004 during the time of investigation, with the uncertainty of the Sr isotope ratios quoted as 2σ. Interference with ^{87}Rb was corrected using a $^{87}Rb/^{85}Rb$ ratio of 0.386. Within-run mass fractionation was corrected for $^{86}Sr/^{88}Sr = 0.1194$.

4 Results

4.1 Petrographic description of dolomites

Fig. 2 shows the distribution of the different types of dolomite through the 100-m-thick lower, clay-rich interval of the Travenanzes Fm., above which the facies switches sharply to massive, bedded dolomites similar to those of the overlying Dolomia Principale. Macroscopically, three types of dolomite can be distinguished: homogenously bedded

dolomite, laminated dolomite, and nodular dolomite (Fig. 3a-c). The lower and middle part of the clay-rich ~~series harbours~~ mainly homogeneous dolomite beds in red clay. Between 40 and 70 m several horizons with gypsum nodules occur (Fig. 3d). A 30-cm-thick fluvial conglomerate with dolomite-cemented quartzarenites and pebbles of ripped up micritic carbonate occurs at 75 m (Fig. 3e), above which palaeosols with dm-scale vertical peds, possible root traces showing green reduction haloes, and nodular dolomite (calcic vertisols; cf. Cleveland et al., 2008), are more frequent (e.g., Fig. 3b). Tempestite beds with megalodonts, foraminifers and ostracods occur at 65 and 89 m. A pronounced transition occurs in the uppermost ca. 8 metres of the clay-rich interval (Fig. 2b), where the clay entirely changes from red to grey colour (Fig. 2c), and laminated dolomites become ~~pre~~dominant while evaporites and palaeosols are absent. The laminated dolomites (Fig. 3c) and cm- to dm-scale dolomite-clay interlayers show intense slumping and soft sediment deformation and pseudo-teepee structures (Figs. 3f, g). ~~Here we provide a~~ short summary of ~~the~~ petrographic analysis of thin sections of the different types of dolomite ~~with~~ the most important features compiled in table 1.

Homogenous dolomites

Homogeneous dolomite beds are usually 10 cm to 50 cm thick, embedded within clays and ~~with~~ sharp, plane-parallel joints. They consist of dolomicrite, which was described as aphanotopic dolomite by Breda and Preto (2011), according to the extended nomenclature for dolomite fabrics by Randazzo and Zachos (1983). The sediment is matrix-supported and contains irregular, partially rounded mud clasts (intraclasts) that consist of ~~an~~ aphanotopic dolomite ~~as the matrix~~. Some of the mud clasts contain smaller and somewhat darker mudclasts or peloids (Fig. 4a, arrow). Soft sediment deformation is often not clearly visible due to the homogeneous structure of the mud, but it can be observed where the mud clasts are deformed within the matrix (Fig. 4b). Some of the homogeneous beds in the lower part of the

312 section show sub-millimetre lamination that is only visible under the microscope, where it
313 ~~appears as an alternation~~ of light (locally coarser) and dark aphanotopic dolomite.
314 The clay content in the homogeneous beds is generally low. A few beds (e.g. at 33.5 m in
315 the section) consist of silty or sandy dolomite, as reflected in a high abundance of detrital
316 quartz in thin section. Pseudomorphs after gypsum occur in a dolomite bed at 120 m (Fig. 4c,
317 d). Moldic porosity occurs ~~in three~~ layers at 43, 65 and 89 m~~, within aphanotopic dolomite~~.
318 These ~~are~~ the tempestite beds observed in ~~the~~ outcrop (cf. Breda and Preto, 2011).
319 One homogenous dolomite bed located at 64 m in the section contains oolit~~h~~ic grainstone,
320 lacking both an aphanotopic and a cement matrix (Fig. 4e). Ooids are either hollow (where
321 the cores may have been dissolved) or filled with sparite and are surrounded with an
322 isopachous cement rim.
323
324 *Nodular dolomites*
325 Nodular dolomites (Fig. 3b) often occur in beds of vertical peds linked to palaeosols as
326 indicated by horizons of ~~typical~~ vertical cracks showing green alteration fronts. Single
327 nodules ~~also may~~ sporadically occur embedded within metre-thick beds of red and green clay.
328 Nodules are usually 5 to 10 cm in size, consist of aphanitic dolomite or occasionally
329 somewhat~~e~~ coarser microspar, and in cross section show both red and pale areas. Most
330 nodules also show a deformed or brecciated internal structure with the interstices between the
331 clasts mostly consisting of matrix and clay cutans.
332
333 *Laminated dolomites*
334 Laminated dolomites occur in the upper part of the clay-rich interval, between 90 and 110
335 m in the section (Fig. 4f-i). In the field, the~~y~~ show an alternation ~~of~~ light grey dolomite
336 laminae and dark grey to black clay laminae ~~in the mm range~~. Some dolomite laminae ~~show~~
337 ~~upward bending~~ reminiscent of pseudo-teepee structures (Fig. 4f)~~, and~~ the space within the

teepee is sometimes infilled with sparry cement. ~~Also,~~ the bending of the laminae towards the upward directed cuspids is reminiscent of load structures (dish structures), but they also may represent desiccation cracks. The laminae are frequently ripped apart and fragments of laminae occur reworked as flat pebbles embedded in an aphanotopic dolomite matrix (Fig. 4g). Some laminae show a microsparitic appearance and laminar fenestral porosity. In some laminae a peloidal fabric is observed (e.g in Fig. 4f). Laminae are typically graded, whereby the upper part is darker, indicating an increase in the clay content (Fig. 4h, i). The top of the laminae is often truncated by an erosion surface, and rip-up clasts of the fine mud ~~(mud clasts)~~ are embedded in the overlying coarse layer. Some laminated dolomites contain continuous layers with inclusions of celestine crystals in the 100-µm-range, some of them with barite in their centre (Fig. 5a-c). Occasionall~~y also~~ pyrite occurs.

Under the SEM, laminated dolomites show an anhedral structure in the 1-5 µm range. No difference in mineral structure and grain size is ~~usually~~ observed between mud clasts and the surrounding, often lighter-coloured matrix. Dolomite crystals at the margins between dolomite and clay interlayers often coalesce into 5-µm-scale round aggregates consisting of several subhedral crystals with different orientation (Fig. 6a, b; the crystals show orientation contrast under BSE mode). Dolomite crystals are often porous, showing a somewhat disordered appearance, but they are surrounded by syntaxial rims. In most cases, the rims entirely fill the intercrystalline space, forming almost hexagonal compromise boundaries (Fig. 6c, d). These rims occur both in homogeneous and laminated dolomites.

Germanic Keuper dolomites

A sample from the Carnian Lehrberg Beds (middle Lehrberg bed; clay pit Friedland, 12 km south of Göttingen, Northern Germany; Seegis, 1997; Arp et al., 2004) ~~shows~~ a brittle structure with high porosity. The material consists mainly of packed ooids or rare~~ly~~ peloids in

363 a sparitic cement matrix. Under the SEM, subhedral to euhedral dolomite in the 5-µm-range
364 are observed within the ooids (not shown).

365 A sample from the Norian Arnstadt Fm. (formerly termed "Steinmergelkeuper"; middle
366 grey series; locality of Krähenberg, 11 km SSW of Göttingen, Northern Germany; Arp et al.
367 2005) shows ~~a~~ mm-scale lamination and cm- to dm-sized laminated clasts, which were
368 interpreted as a stromatolite breccia. The laminae contain abundant agglutinated siliciclastic
369 grains (mainly quartz, subordinate albite) and phosphoritic fish scales. The dolomicrite ~~shows~~
370 a subhedral structure in the ≤5 µm range with a few larger subhedral grains resulting in a
371 porphyrotopic fabric ~~(not shown)~~.

372

373 **4.2 Mineralogy**

374 Bulk dolomite shows a position of the 104 peak at a mean d-value of 2.88816 Å (Fig. 7a;
375 Table 2). This indicates a Ca content of 50.7%, based on the equation of Lumsden (1979).
376 The structural order is indicated by the ratio of the superlattice-ordering peak at (015) to the
377 (110) ordering peak. The height ratio is 0.44, which is near ~~to~~ 0.519 (Table 2) indicated for an
378 ordered dolomite in the Highscore database.

379 Clay mineral analysis (Fig. 7b-d) revealed illite in samples TZ14-1 and TZ14-7 and an R3
380 ordered illite-smectite mixed-layer clay mineral in sample TZ14-9. In the ethylene-glycol-
381 saturated state, the broad shoulder at 11.4 Å contains components of the illite 001 reflection
382 and of the fourth order of a 47 Å superstructure peak whose unit cell consists of three 10 Å
383 illite layers and one 17 Å smectite layer (Moore and Reynolds, 1997). This smectite
384 component ~~was~~ not observed in samples TZ14-1 and TZ14-7.

385

386 **4.3 Carbon content**

387 Total carbon contents in shales (Table 3) range from 0.06 to 0.51 wt%. Samples TZ16-1
388 und TZ16-19B showing the lowest TIC of 0.02 wt% were selected as controls to test for

389 $^{87}Sr/^{86}Sr$-ratios of Sr potentially adsorbed to clay minerals. TOC-contents are in the range of
390 0.05 - 0.16 wt%. Max. TIC-values are 0.46 wt%.
391
392 **4.4 Carbon and oxygen isotopes**
393 Carbon isotope values vary between -3.38 and +4‰ VPDB. Oxygen isotope values are
394 between -0.7 and +0.9‰ VPDB (three outliers show values as low as -1.5‰ VPDB; Table 4;
395 Fig. 8a). A clear distinction occurs between nodular dolomites ~~showing~~ negative $\delta^{13}C$-values
396 and homogeneous dolomites showing positive values. Laminated dolomites ~~show~~
397 intermediate values and low variability. The oxygen isotopes show an upward increasing
398 trend (Fig. 8b). The calculated temperature of formation assuming a Triassic seawater
399 composition of -1‰ VSMOW using the fractionation equation of Vasconcelos et al. (2005)
400 ~~shows~~ temperatures between 29 and 39°C~~. A~~ more positive value ~~of the water~~ would result in
401 higher temperatures.
402
403 **4.5 Element composition of the dolomites**
404 Concentrations of ~~the elements~~ Al, Ca, Fe, K, Mg, Mn, Na, P, Ti, Ba, Sr, and Rb (mmol/g
405 sample) are shown in Table 5. Ca contents are between 1.68 and 2.33 mmol/g in the 0.1 N
406 acetic acid fraction and between 2.71 and 2.87 mmol/g in the 1 N acetic acid fraction. Mg
407 contents are between 1.61 and 2.34 mmol/g in the 0.1 N acetic acid fraction and between 2.48
408 and 2.64 mmol/g in the 1 N acetic acid fraction. Based on these concentrations, the amount of
409 dolomite dissolved is between 30 and 43 wt% of the bulk sample in the 0.1 N acetic acid
410 fraction and between 49 and 52 wt% in the 1 N acetic acid fraction of the sequential
411 extraction. In total, between 84 and 90 wt% of the bulk sample were dissolved during these
412 two extraction steps. If molar concentrations of Ca are plotted vs. Mg a linear trend with a
413 slope of 0.935 is observed (Fig. 9a), indicating 48.3 mol% $MgCO_3$ in the dolomite phase.

The Sr-concentrations in bulk dolomite samples are in the range of 0.38 and 1.16 µmol/g in the 0.1 N acetic acid fraction and between 0.57 and 0.79 µmol/g in the 1 N acetic acid fraction (except one extremely high value of 34.91 µmol/g in sample TZ14-9). These contents are much higher than in pure clay mineral samples with 0.047-0.417 µmol/g in the 0.1 N acetic acid fraction and even lower concentrations (<0.19 µmol/g) in the other fractions. In all samples measured by ICP-OES, rubidium (Rb) concentrations are below the detection limit of 0.012 µmol/g.

Correlation of Sr contents to other elements did not show clear trends. In particular, Sr-content did not correlate with Mg or Ca. Sr correlates with K (Fig. 9b), but at the same time, K is extremely low in all clay mineral leachates.

4.6 Sr-isotopes

$^{87}Sr/^{86}Sr$-ratios of pure minerals

Results of Sr-isotope measurements are listed in Table 6. Repeated extractions of chemically pure dolomite reference material dissolved in 0.1 N acetic acid showed a range of $^{87}Sr/^{86}Sr$-ratios between 0.709942 ±0.000011 and 0.710831 ±0.000007. Pure single crystals of dolomite extracted sequentially showed the highest value (0.708401 ±0.000040) in the 1 M NaCl fraction. Values in the 0.1 N acetic acid fraction (0.707735 ±0.000006) and the 1 N acetic acid fraction (0.707666 ±0.000006) are lower by almost 0.001 than in the NaCl fraction.

In pure barite, $^{87}Sr/^{86}Sr$-ratios decrease by about 0.0013 in the extraction sequence from 0.1 N acetic acid to 6 N HCl. Celestine is highly soluble and was only measured in the 1 M NaCl fraction and one time in 0.1 N acetic acid. It shows similar values as in the 1 M NaCl fraction of the pure barite-celestine-dolomite mixture (0.708038 ±0.000003), but the latter increased to 0.709501 ±0.000040 in the 0.1 N acetic acid fraction.

439

440 *$^{87}Sr/^{86}Sr$-evolution during sequential extraction of dolomites of the Travenanzes Fm.*

441 Different modifications of the sequential extraction were investigated using three samples
442 (TZ14-1, TZ14-7 and TZ14-9; Table 6). $^{87}Sr/^{86}Sr$-ratios decrease in sample TZ14-1 from
443 0.708125 ±0.000012 to 0.707666 ±0.000004 with increasing strength of the leaching reagent,
444 while the values remain almost constant in sample TZ14-9. However, repeating the 0.1 N
445 acetic acid extraction (for 36 h) after a rather intense first extraction (4h, 12h, 4h) resulted in
446 extremely high values (0.715417 ±0.000250 in TZ14-1 and 0.7192266 ±0.000455 in TZ14-9).
447 Standard deviations are also higher than in the other fractions.

448 The sequential extractions were repeated, whereby the Sr-concentrations were determined
449 by ICP-OES (see section above). In addition, 1 N acetic acid and 6 N HCl fractions were
450 extracted. Results are similar to the previous extraction sequences, but the values further
451 decreased in the 1 N acetic acid fraction. Only the HCl-fraction showed very high values of
452 0.730453 ±0.000005 in sample TZ14-7.

453 Sequential extractions of the clay samples from the Travenanzes Fm. show a similar
454 increase with the sequential extraction steps from 0.1 N acetic acid fraction to 6 N HCl, where
455 $^{87}Sr/^{86}Sr$-ratios reach similar values as in the dolomite extracts (from 0.722998 ±0.000018 to
456 0.733910 ±0.000024).

457

458 *$^{87}Sr/^{86}Sr$-ratios in micro-drilled dolomite*

459 Eleven dolomite samples were micro-drilled from areas where dolomite was most pure
460 based on examination by SEM and dissolved in 0.1 N acetic acid. The values of the
461 Travenanzes Fm. are in the range of 0.707672 ±0.000003 to 0.707976 ±0.000004. The highest
462 value occurs in a dolomite nodule, while no systematic difference between homogenous and
463 laminated dolomite was observed. Dolomite of the Germanic Keuper samples shows much
464 higher $^{87}Sr/^{86}Sr$-ratios of 0.709303 ±0.000006 and 0.709805 ±0.000005, respectively.

465

466 *$^{87}Sr/^{86}Sr$-ratios of modern dolomites (Deep Springs Lake, Coorong Lakes)*

467 Dolomites of Deep Springs Lake show strongly radiogenic values of 0.713086 ±0.000004
468 and 0.713207 ±0.000004, which are much higher than modern seawater values, ~~showing~~ a
469 $^{87}Sr/^{86}Sr$-ratio of 0.709234 ±0.000009 (DePaolo and Ingram, 1985). In contrast, dolomite from
470 the Coorong Lakes (Milne Lake) ~~shows~~ ratios between 0.709251 ±0.000004 and 0.709275
471 ±0.000003, which is very near to modern seawater. Different incubation times (5 min und 10
472 h) in 0.1 N acetic acid had no influence on the isotope ratios.

473

474 **5 Discussion**

475 **5.1 Interpretation of microfacies within different types of dolomite**

476 *Homogeneous dolomite beds*

477 The homogeneous dolomite beds, which are mainly intercalated in the lower, clay-rich part
478 of the Travenanzes Fm., consist of fine-grained dolomicrite (aphanotopic dolomite), with
479 occasional intraclasts of the same aphanotopic dolomite ~~as the matrix~~. Soft sediment
480 deformation and dolomicrite infill between mud clasts indicate that this sediment consisted ~~to~~
481 ~~a large extent~~ of unlithified carbonate mud. Based on the abundance of fine mud, water
482 energy was probably not very high (Demicco and Hardie, 1994), although reworking and
483 partial rounding of the mud clasts require at least occasionally higher water energies.
484 According to the standard microfacies concept this type falls into SMF 23 (“non-laminated
485 homogeneous micrite and microsparite without fossils”), indicating ~~a~~ deposition in “saline
486 and evaporative environments, e.g. in tidal ponds” (Flügel, 2010). ~~Also~~, SMF 24 (“lithoclastic
487 floatstones, rudstones and breccias”) is observed in some of the beds where mud clasts are
488 abundant. These facies types are consistent with supersaturation-driven precipitation of ~~a~~ fine-
489 grained authigenic carbonate in environments partially restricted from open seawater and
490 would match ~~both~~ with a coastal sabkha environment and/or ~~with~~ shallow ephemeral lake~~s~~.

Ephemeral lakes may have formed on extended coastal alluvial plains along the Tethyan margin during the Carnian. The fine mud may have been homogenized and redistributed due to minor wave action in the ponds (cf. Ginsburg, 1971).

In a semi-arid climate, episodic flooding of the alluvial plains by river water, which however mostly evaporated before reaching the coast, led to the formation of a dryland river system (Breda and Preto, 2011). The fluvial system may have supplied water to temporally existing evaporating ponds. Alternatively, the alluvial plain may have been sporadically flooded by seawater, explaining the intercalations of authigenic dolomite layers in the succession of alluvial clays. Homogeneous dolomites show a positive carbon isotope signature between 0.7 and 4‰ VPDB (except one outlier), which would be consistent with formation from unaltered marine carbon in evaporative brine, with no significant contribution of ^{12}C derived from organic matter. As indication of evaporative conditions, several gypsum beds occur between 45 and 70 m in the section, and pseudomorphs after gypsum were observed in a thin section of a dolomite at 120 m (Fig. 4c, d). But evaporites may not always be preserved as they were most likely dissolved due to seasonally wet conditions.

While most homogeneous dolomite beds consist of aphanitic dolomite, a bed of dolomitic ooid grainstone devoid of matrix occurs at 64 m (Fig. 4e), and tempestites showing moldic porosity indicative of dissolved allochems and dissolved fossils occur at several levels in the section. These beds must represent events of higher water energy, contributing sediment from more open marine areas. The presence of marine fossils, such as *Megalodon*, indicate that at least episodically the environment was marine influenced. The microfacies of the oolite falls into SMF 15, which indicates proximity to the seaward edge of the platform. A similar facies, however, is encountered in the Carnian Lehrberg Beds (Seegis, 1997) in a lacustrine setting. Several beds containing abundant siliciclastic material (mainly angular quartz clasts) are more likely due to a riverine flooding event, providing detrital material from the continent. Thus,

the microfacies in homogenous dolomite beds indicates both marine and continental influence on the depositional environment.

Laminated dolomite

In the upper part of the clay-rich interval, predominantly laminated dolomites reminiscent of loferites (Fischer, 1964) occur. The change from more homogeneous to laminated dolomite intercalations correlates with the change from red to dark grey clay. The lamination consists of millimetre-scale dolomite/clay interlayers suggesting an alternation of clay and fine dolomite deposition. The microfacies falls into SMF 25 ("laminated evaporite-carbonate mudstone facies") indicating an "upper intertidal to supratidal sabkha facies in arid and semiarid coastal plains and evaporitic lacustrine basins" (Flügel, 2010). Laminae showing soft sediment deformation could not be attributed to stromatolitic bindstone facies (SMF 19 to 21). Only some layers showing a coarser fabric with interstitial dolosparite or dolomicrosparite containing putative peloids have been interpreted as microbial laminites (Preto et al., 2015). Mostly, graded bedding indicates a direct sedimentation process rather than in situ precipitation of the primary carbonate within a microbial mat (Vasconcelos et al., 2006; Bouton et al., 2016; Court et al., 2017; Perri et al., 2018). A detrital origin of the clay in the dolomites is confirmed by the well-ordered illite-smectite mixed-layer composition which would be atypical for authigenic clay minerals. Frequent subaerial exposure and desiccation may explain why the sediment was not homogenized and the lamination is preserved. This is supported by the occurrence of pseudo-teepee structures as remnants of desiccation cracks. Rip-up clasts were formed during subsequent flooding, whereby angular flat pebbles occur where the sediment was desiccated or partially lithified. However, laminae also show frequently plastic deformation (e.g. in Fig. 3g) where the mud was still unlithified.

Some uncertaintly exists as to whether the facies was peritidal or represents ephemeral lakes, as suggested for the homogeneous dolomites above. Episodic high water-energy

indicated by the rip-up clasts, combined with frequent desiccation, could point to evaporative tidal conditions~~, as they~~ occur in a sabkha. What is atypical for a modern sabkha is the large amount of detrital input. ~~But this is owed~~ to ~~the~~ seasonally wet conditions during the Carnian and the ~~facies~~ can be considered a mixed facies of alluvial plain and coastal sabkha: a "dirty" sabkha. Under such conditions, ~~the~~ large amounts of evaporites, in particular gypsum, ~~as they usually occur in a sabkha,~~ could have been dissolved. Why the occurrence of laminated dolomites coincides with the transition from red to grey clays is not clear but may be related to more permanently water-saturated conditions in the subsurface, while the surface was exposed to periodic desiccation. ~~Also this would~~ be consistent with a sabkha environment.

Nodular dolomite

The clay beds were subject to strong evaporation and vadose diagenesis causing oxidation and red colour. This generally indicates~~,~~ at least seasonally~~,~~ arid conditions. Dolomite nodules that occur sporadically within certain intervals show internal brecciation, which probably occurred after sedimentation. Internal brecciation is a typical feature of present day calcretes in arid environment (e.g. Mather et al., 2018). Slightly negative $\delta^{13}C$-values indicate a contribution of carbon derived from organic matter degradation, suggesting that they formed within the sediment. ~~Presumably~~ the formation of dolomite nodules could be related to diagenesis in palaeosols. In the upper part of the section (between 80 and 105 m) dolomite nodules are associated with green reaction haloes along vertical peds in palaeosols of vertisol-calcisol type (Preto et al., 2015). Carbonate formation may have been related to reducing fluids in water-logged soils during humid intervals, while the crack formed during desiccation in dry periods, perhaps facilitated by the presence of expandable clay minerals (smectite).

5.2 The origin of ionic solutions conducive to dolomite formation

Overall, the dolomites in the Travenanzes Fm. show facies that match a variety of potential

depositional environments. They ~~show some~~ similarity to the Germanic Keuper, and it is not entirely clear ~~from the facies, whether~~ a marine influence occurred, except ~~if~~ indicated by marine fossils, as in the tempestite beds. ~~To~~ better trace the origins of ionic solutions to the environments that were conducive to dolomite formation~~, Sr-isotopes were analysed.~~

Strontium derived from seawater

Radiogenic $^{87}Sr/^{86}Sr$ ratios can be indicative of the source of ionic solutions ~~from which~~ the dolomite precipitated (Müller et al., 1990a; Müller et al., 1990b). Sr-isotopes in selected dolomites ~~through~~ the Travenanzes Fm. at the Dibona section show~~ed~~ values between 0.707672 ±0.000003 and 0.707976 ±0.000004. We correlate the Dibona section (Fig. 10) with the Carnian seawater curve (Korte et al., 2003)~~.~~ ~~A~~lthough the age interval of the Travenanzes Fm. is not precisely constrained, ~~findings of ammonites~~ at the base of the succession suggest a Tuvalian II age (*subbullatus* zone, 232.5-231.0 Ma; Ogg, 2012). The upper boundary of the Travenanzes Fm. is time-transgressive and hence the age not precisely constrained. We assume that the sedimentation rate was at least as high, or higher, than in the peritidal carbonates of the Dolomia Principale. In this region, the Dolomia Principale includes a part of the Rhaetian (Neri et al., 2007) and, thus, its upper boundary is near the Triassic-Jurassic boundary at 201.3 Ma. The seawater curve was fixed at the lower boundary of the Travenanzes Fm. and the time axis was varied to fit the seawater curve parallel to the envelope of minimal $^{87}Sr/^{86}Sr$-ratios measured in the dolomites (Fig. 10). The base of the first massive dolomite at 110 m in the profile would ~~then~~ have an age of approximately 229 Ma.

Comparison with the seawater curve shows that the dolomites of the Travenanzes Fm. have largely marine $^{87}Sr/^{86}Sr$-ratios (Fig. 10). Only values from micro-drilled samples ~~most gently~~ extracted with 0.1 N acetic acid were used for this reconstruction, and the resulting values all lie within ~~a range of~~ 0.00022 ~~with the~~ seawater values (grey shaded area). This scatter towards more positive values, compared to seawater, may be due to a small influence ~~of~~

continental water. Indeed, during deposition of the Travenanzes Fm. sufficient continental water would have been available from rivers, and ions may have become concentrated while the water was evaporating in the distal alluvial plain. Alternatively, Sr desorbed from clay minerals could have added more radiogenic values to the brine. But even if a small influence of Sr of continental origin is present, ~~because of the much higher Sr concentrations in seawater,~~ the marine signal is dominant.

This observation does not support the classical Coorong model for dolomite formation, where alkalinity is largely derived from continental groundwater. The Coorong Lakes in South Australia are ephemeral lakes largely supplied ~~with~~ groundwater (Von der Borch et al., 1975). Strangely, ~~though,~~ the $^{87}Sr/^{86}Sr$ ratios we measured ~~in~~ Milne Lake (one of the Coorong Lakes) ~~show~~ modern seawater composition (Fig. 11), but this can be explained as the local groundwater largely originates from a Pleistocene carbonate aquifer, accordingly carry~~ing~~ a Pleistocene Sr-isotope signature. A similar scenario for the Travenanzes Fm. is unlikely as the only large-scale preceding carbonate platforms at that time were the ~~Late~~ Ladinian-Carnian Cassian dolomite platforms (Russo et al., 1997). B~~ut b~~ased on the stratigraphic context, all basins between these platforms were infilled by the Heiligkreuz Fm. and an extremely flat topography ~~had~~ established that ~~was~~ stratigraphically overlain and sealed by the alluvial deposits of the laterally persistent Travenanzes Formation. Furthermore, the Travenanzes Fm. consists of 100 m of impermeable clay (~~containing~~ expandable clays) such that ~~a~~ long-distance transport of groundwater can be excluded.

We conclude that the $^{87}Sr/^{86}Sr$ ratios of the dolomites ~~truly~~ represent a ~~dominating~~ marine influence. Presumably, seawater was transported to the interior of the platforms by episodic flooding (spring tide or storm) events. Even in a seasonally wet climate the input of river water on Sr-isotopes was insignificant compared to the influence of ions (including Sr) from seawater that ~~became~~ concentrated by evaporation. Laminated dolomites in the uppermost part of the section show values most similar to seawater composition, which is consistent with

620 a greater influence of peritidal conditions.

621

622 *The influence of Sr adsorbed to clay minerals*

623 An outlier with higher $^{87}Sr/^{86}Sr$ ratios occurs in a dolomite nodule, presumably representing
624 a more continental influence or perhaps more seasonally wet and evaporative conditions with
625 less marine influence. But ~~also~~ higher values may be due to contamination and partial
626 leaching of clay minerals within the dolomite samples. Within the extraction sequence (1 M
627 NaCl → 0.1 N acetic acid → 1 N acetic acid), the $^{87}Sr/^{86}Sr$ ratio generally remains constant or
628 becomes slightly less radiogenic, i.e., more similar to seawater. However, the values strongly
629 increase with leaching in 6 N HCl (Table 6). A modification of ~~the~~ $^{87}Sr/^{86}Sr$ ratios due to
630 contamination by ^{87}Sr from the radioactive decay of ^{87}Rb to ^{87}Sr can be considered as
631 negligible since the concentrations of Rb was below the detection limit of 0.05 ppm (Table 5)
632 and the half ~~time of the decay~~ is 48.8 billion years. ~~Also, an~~ influence of celestine and Sr-rich
633 barite, observed under ~~the~~ SEM, on ~~the~~ Sr-isotope values can be largely excluded. These
634 mineral phases are bound to distinct layers of the laminated dolomites, ~~where~~ they could be
635 avoided by micro-drilling ~~in~~ areas where the dolomite ~~was~~ pure. Only one value ~~in~~ sample
636 TZ14-9 shows extremely high Sr-concentrations. This sample was micro-drilled near ~~to~~ a
637 celestine layer and it is therefore not surprising that a celestine crytal may have been ~~leached~~.
638 The isotopic composition of the celestine is also similar to Carnian seawater.

639 In the NaCl-fraction only minimal amounts of dolomite are dissolved. The slightly more
640 radiogenic $^{87}Sr/^{86}Sr$ ratio may be derived from Sr that is lightly adsorbed to clay minerals and
641 finely dispersed in the clay matrix, although Sr^{2+} as a two-valent cation is more strongly
642 adsorbed to clay mineral than Na^{+}, and thus not easily desorbed by NaCl. ~~With increasing~~
643 ~~extraction efficiency and purity of the carbonate phase, t~~he values approach seawater values
644 in the 1 N acetic acid fraction. ~~Also, v~~alues from micro-drilled samples are generally more
645 similar to seawater values, probably because more pure dolomite was sampled (Table 6). 1 N

acetic acid is usually observed ~~not to~~ strongly attack interlayer ions in clay minerals.

Clay minerals leached in 6 N HCl show significantly more radiogenic values compared to dolomite samples (Table 6). This finding is consistent with strongly radiogenic values in the 6 N HCl-fraction of dolomite samples (up to 0.730453 ±0.000005) and supports that the clay minerals are the carriers of a Sr-pool significantly more radiogenic than the carbonate phase showing marine values. Sr is known to adsorb to illite-smectite mixed layer clay minerals (Missana et al., 2008). The HCl-fraction most likely includes adsorbed Sr~~,~~ and Sr occupying the interlayer positions of the clay minerals, and presumably also structurally bound Sr in the clay mineral phase. In particular, illite-smectite mixed-layer clay minerals, as detected by XRD of the clay mineral separate in sample TZ14-9 (Fig. 7d), could have two different origins~~,~~ burial diagenesis and continental weathering. Based on the tectonic setting and ~~low~~ burial depth of the Dolomites, burial depth for smectite-illite transition has not been reached. Therefore, these minerals are most likely derived from silicate weathering, with the Sr-signature representing the crustal origin of the parent rock. Our finding of radiogenic Sr-isotope ratios supports that clay minerals did not ~~essentially~~ incorporate ~~the~~ Sr from seawater~~,~~ ~~delivered at~~ high sealevel stand. It is therefore clear that Sr extracted from the dolomites is not derived from clay minerals.

Dolomite as primary archive of Sr-isotope signatures

The question is~~,~~ whether Sr truly represents the conditions of dolomite formation or whether it ~~inherits~~ the Sr content of some precursor phase. Baker and Burns (1985) and Vahrenkamp and Swart (1990) ~~showed~~ very small distribution coefficients between aqueous and solid solutions, and high Sr-contents measured in Abu Dahbi sabkha dolomites (Müller et al., 1990b) may be derived from precursor aragonite. However, dolomite in the Travenanzes Fm. is largely primary (Preto et al., 2015) and thus not formed from an aragonite precursor. It is likely that remobilization of Sr during burial may have released ~~parts of the~~ Sr from

672 dolomite ~~which~~ is now present as celestine and barite inclusions.

673 Furthermore, Sánchez-Román et al. (2011) demonstrate~~d~~ that protodolomite forming in
674 culture experiments contain Sr in the range of several thousand ppm. The incorporation
675 mechanism of Sr is still not entirely clear, since Sr is a large ion that should occupy the sites
676 of Ca in the crystal lattice. However, in Sánchez-Román et al. (2011) Sr appears to correlate
677 with the Mg content, and another incorporation mechanism may occur, such as ~~by~~ surface
678 entrapment. A correlation of Sr-contents with K-contents is observed for the Travenanzes
679 dolomites. It could be circumstantial, but would not be inconsistent with an alternative
680 mechanism of Sr-incorporation, such as surface entrapment. Even if ~~it is taken into account~~
681 ~~that~~ only protodolomite formed in microbial culture experiments (Gregg et al., 2015), natural
682 modern dolomites are often rich in Sr (e.g. Meister et al., 2007). The Sr could occur in
683 disordered nano-structural domains that are not picked up in the bulk XRD-signal.
684 Alternative, non-classical nucleation and growth pathways, e.g. by nano-particle attachment,
685 could play a role in the abnormal partitioning of Sr in the dolomite lattice. Thus, a high Sr-
686 content in the Travenanzes Fm. or in Abu Dhabi Sabkha dolomites is likely a true signature of
687 primary dolomites.

688

689 **5.3 Mode of dolomite formation and comparison with known models**

690 *Primary dolomite formation*

691 Several ~~indications~~ support ~~that the~~ origin of dolomite in the Travenanzes Fm. ~~is largely~~
692 ~~primary~~. Formation temperatures reconstructed from oxygen isotopes ~~and~~ assuming Triassic
693 seawater composition of -1‰ VSMOW are between 28 and 33°C. If a typical ^{18}O enrichment
694 of 3‰ in a sabkha ~~(McKenzie et al., 1980; McKenzie, 1981)~~ is assumed, the calculated
695 temperatures ~~would be~~ between 40 and 50°C, which is still within ~~a~~ range ~~possible~~ in a
696 sakbha. Both temperature and evaporation may have changed over time, which may explain
697 the observed linear trend in oxygen isotopes across the section (Fig. 8B). Furthermore, there is

698 no co-variation between $\delta^{13}C$ and $\delta^{18}O$, as opposed to evaporation in hydrologically closed
699 settings such as the Germanic Keuper basin (Reinhardt and Ricken, 2000; Arp et al., 2005).
700 Both oxygen isotopes and nano-crystalline structures observed by Preto et al. (2015) preclude
701 a later pervasive recrystallization during burial diagenesis. Sedimentary structures indicate
702 that most of the homogenous dolomite and laminae containing aphanotopic dolomite was
703 unlithified, and dolomite was therefore deposited as fine-grained mud. This is further
704 supported by mm-scale interlayering of clay and dolomite in the laminated dolomites near the
705 top of the sequence, and some dolomite/clay couplets ~~showing a~~ fining-upward bedding.
706 Based on the observation of nano-crystal structures, replacement did not take place and it
707 appears logical to assume that the primary phase was already dolomite.

708 While most of the dolomite may have been primary, micron-scale interstices between the
709 dolomicrite grains must have been cemented after deposition. This cementation resulted in
710 rims visible under ~~the~~ SEM and result~~ing~~ in near hexagonal compromise boundaries. The
711 cement may have contributed ^{13}C-depleted carbon during early diagenesis. The lowest $\delta^{13}C$
712 values of -3.4‰ VPDB occur in the nodules. There is no indication that these nodules formed
713 at the surface. They rather formed within the sediment, probably due to reducing conditions
714 and influenced by dissolved inorganic carbon from degrading organic matter in the
715 palaeosols. Homogeneous and laminated dolomites are clearly distinct from nodules in their
716 carbon isotope compositions (Fig. 8a), indicating only a minor contribution from pore-water
717 derived dissolved inorganic carbon. Carbon isotope values are thus largely consistent with ~~a~~
718 primary precipitation. The mode of dolomite formation as fine mud and subsequent
719 cementation is comparable to several modern sites of dolomite formation.

720

721 *The sabkha model*

722 The classical sabkha model involves dolomite formation under intra-supratidal conditions,
723 concentration of brines through either seepage reflux (Adams and Rhodes, 1960) or

724 evaporative pumping (Hsü and Siegenthaler, 1969; Hsü and Schneider, 1973; McKenzie et
725 al., 1980; McKenzie, 1981) and precipitation of dolomite ~~upon increase of the~~ Mg/Ca ratio
726 due to gypsum precipitation (see Machel, 2004, for a more detailed discussion of varieties of
727 sabkha models). ~~This group of models allow~~ for a mixture of seawater and continental
728 groundwater, with seawater providing ~~mainly~~ the ions for dolomite precipitation. Coastal
729 sabkhas are typically characterized by laminated (Lofer-type) dolomites, where~~by~~ the laminae
730 are largely ~~still~~ unlithified after deposition (Illing, 1965; Bontognali et al., 2010; Court et al.,
731 2017). In ~~fact, in~~ the sabkha of Abu Dhabi, both pathways, via replacement of precursor
732 aragonite and by direct precipitation of dislocation-ridden primary dolomite, ~~we~~re observed
733 (Wenk et al., 1993).

734 The sabkha model is thus a reasonable model for the uppermost parts of the Travenanzes
735 section, ~~showing~~ laminated dolomites, marine Sr-isotope values and indications of frequent
736 desiccation and flooding in a peritidal setting. Yet, the conditions differ~~ed~~ from the modern
737 sabkhas along the Persion Gulf ~~by~~ the large amount of alluvial clay (dirty sabkha), as opposed
738 to aeolian sand. Most of the fine lamination ~~then~~ may result from periodically varying
739 conditions, perhaps with clay deposition during episodes of fluvial discharge and carbonate
740 deposition during evaporative conditions.

741

742 *The continental playa lake model*

743 The playa lake model was originally suggested by Eugster and Surdam (1973) for dolomite
744 of the Green River Formation (Wyoming), but the primary formation of fine dolomite mud is
745 observed in many alkaline playa lakes, such as Deep Springs Lake (Peterson et al., 1963;
746 Clayton et al., 1968; Meister et al., 2011), Lake Acigöl (Turkey; Balci et al., 2017), Lake
747 Neusiedl (Austria; cf. Neuhuber et al., 2016), Lake Van (Turkey; McCormack et al., 2018; for
748 an overview see Eugster and Hardie, 1978, and Last, 1990). This type of setting has also been
749 suggested for the Germanic Keuper deposits during the late Carnian and Norian, when the

Germanic Basin was entirely disconnected from ~~the~~ Panthalassa ~~ocean~~ and was continental (Reinhardt and Ricken, 2000). The Travenanzes Fm., with its homogeneous dolomite intercalations in red and green clays, is strikingly similar to playa-lake Keuper facies in the Germanic Basin. There, dolomite formed ~~upon~~ evaporation and concentration of the continental brines under semi-arid climate.

~~However,~~ Sr-isotope data support a dominantly marine origin of ionic solutions to the Travenanzes Fm., whereas Sr-isotopes are strongly radiogenic in the Germanic Keuper dolomites (or in Deep Springs Lake; Fig. 11). The two settings are thus fundamentally different. Even dolomite nodules, showing somewhat more radiogenic values than seawater in the Travenanzes Fm., ~~are~~ still indicat~~ing~~ a ~~dominating~~ marine influence. The slightly more radiogenic influence could be due to ~~the~~ clay minerals present in the nodules that were difficult to entirely separate from the carbonate. Also, dolomite nodules may have formed in relation to palaeosols, during somewhat more humid times and, thus, may have been slightly influenced by continental water input from ~~the~~ rivers.

The coastal ephemeral lake model (Coorong model)

The Coorong model was proposed by Von der Borch et al., 1975~~;~~ Von der Borch 1976~~;~~ Rosen et al., 1989~~;~~ see Warren, 2000, for detailed information)~~,~~ explain~~ing~~ the formation of primary and uncemented dolomite in the Coorong lakes of South Australia. The isotope values show that the contribution of ionic solutions, and hence alkalinity, of continental origin to the dolomitizing fluids was minimal and that the dolomites are seawater derived. This may be distinct from the typical Coorong model, where alkalinity is provided from an inland karst system. But other coastal ephemeral lakes exist, ~~such as~~ along the Brasilian coast north of Rio de Janeiro. Partially unlithified dolomite occurs in Brejo do Espinho (Sánchez-Román et al., 2009), which is ~~in fact~~ largely similar to the Coorong lakes, but ionic solutions are ~~largely~~ derived from seawater.

776 A coastal ephemeral lake model would probably be most suitable to explain homogeneous
777 dolomite beds of the Travenanzes Fm., where hypersaline ponds may have formed in a
778 dryland river system. However, unlike ~~the~~ recent ephemeral lakes (such as Lagoa Vermelha,
779 Brejo do Espinho and the Coorong Lakes) the clay-rich sediment must have inhibited
780 groundwater flow. Hence, while modern coastal ephemeral lakes receive their water largely
781 through seawater percolating through porous dune sand, episodic flooding with seawater must
782 have provided ionic solutions for dolomite formation on the Carnian platform.
783
784 *A non-actualistic system*
785 Overall, the depositional environment reconstructed for the Travenanzes Fm. shows
786 similarities to modern systems were dolomite forms. Among all the scenarios, a coastal
787 ephemeral lake model would be most similar to the conditions conducive to homogeneous
788 dolomites, lacking signs of frequent desiccation, while a coastal sabkha model may explain
789 the laminated intervals near the top of the studied succession. In contrast to ~~any~~ modern
790 systems, the clay rich sediments of the Travenanzes Fm. precluded any ~~transport~~ of
791 groundwater, which plays a role for ionic transport in both the modern day ephemeral lake
792 model and the different versions of sabkha models. Although modern systems provide valid
793 analogues for the mechanism of dolomite formation in the past, and probably throughout
794 Earth~~'s~~ history, none of them is an exact environmental analogue. The Carnian alluvial plains
795 that covered an enormous area along the Tethys margin (e.g. Garzanti et al., 1995) represent a
796 non-actualistic system in terms of their sedimentary, hydrological and climatic conditions.
797 ~~Besides,~~ the geochemistry of Tethys seawater may also have been different from today, an
798 issue that requires further investigation. These aspects need to be taken into account if we
799 intend to understand ~~the role of~~ dolomite formation through Earth history.
800 In the light of ~~a possible~~ spontaneous precipitation ~~as~~ fine mud in the water column,
801 perhaps via formation and aggregation of nano-particles, further discussion of a nucleation

and growth pathway of dolomite ~~will be~~ necessary. While several modifiers may also play a role in the water column, such as dissolved organic matter (Frisia et al., 2018), microbial EPS (Bontognali et al., 2013), or suspended clay particles (Liu et al., 2018), fluctuating conditions inducing spontaneous nucleation and growth of dolomite, in agreement with Ostwald's step rule (Deelman, 1999), require further consideration as a factor favourable for dolomite formation on a seasonally variable platform (Meister and Frisia, accepted).

The main finding of this study is that most of the dolomite in the >100 m thick Travenanzes Fm. probably formed through direct precipitation ~~in~~ a seawater-derived solution. This mode of primary dolomite formation has rarely been considered in the study of ~~geological dolomite bodies~~, but may explain the genesis of many other large-scale, fine dolomite units that preserve fossils and sedimentary structures.

6 Conclusions

Dolomite beds intercalated in a 100-m-thick Carnian alluvial clay sequence in the Travenanzes Fm. largely formed as fine-grained primary mud. The depositional environment was minimally affected by currents and most likely prevailed as ephemeral lakes in an extended alluvial plain or dryland river system. The large amounts of clay are related to at least seasonally wet conditions~~. Also~~ palaeosols and diagenetic dolomite nodules could have formed under such conditions. The facies resembles ~~strongly~~ those of ~~the~~ Triassic playa lakes ~~prevailing~~ in the Germanic Basin or in the modern Deep Springs Lake.

Sr-isotopes clearly show a marine signal, indicating seawater as the main source of ions. The depositional environment ~~shows most similarities with~~ coastal ephemeral lakes resulting in the deposition of homogeneous dolomite beds through most of the sequence, changing into a "dirty" sabkha near the top of the sequence, where fine dolomite/clay interlayers suggest alternating deposition of extremely fine authigenic dolomite from evaporating water, and clay.

828 Overall, Sr-isotopes and petrographic observations provide insight into a non-
829 uniformitarian system including ~~both~~ elements of coastal ephemeral lake systems and sabkhas
830 as ~~an~~ environment of primary dolomite formation. Considering the precipitation of primary
831 dolomite from coastal lakes or ponds may help explain~~ing~~ other dolomite deposits with
832 preserved sedimentary features throughout geologic history.
833
834 *Acknowledgements*. We thank C. Beybel, I. Wünsche, and L. Slawek for preparing high-
835 quality petrographic thin sections. Thanks also to W. Obermaier for analysing element
836 concentrations by ICP-OES and P. Körner for support during TOC measurements. S.
837 Niebergall provided some of the petrographic images. We furthermore thank S. Viehmann for
838 help during sampling and supervision of the students in the field and B. Bethke for her strong
839 support in the laboratory. Thanks also to M. Lorencak for the help during sampling of
840 dolomite from the Coorong Lagoon. We thank S. Frisia for input and constructive criticism.
841 F. Franchi and H. Machel reviewed an early version of this manuscript. The study was
842 partially supported by the Marie Curie Intra-European Fellowship Project Triadol (Project no.
843 626025).
844
845 **References**
846 Adams, J.E., and Rhodes, M.L.: Dolomitization by seepage refluxion, Am. Assoc. Petrol.
847 Geol. Bull., 44, 1912–1921, 1960.
848 Alderman, A.R. and Skinner, H.C.W.: Dolomite sedimentation in the South-East of South
849 Australia, Am. J. Sci., 255, 561–567, 1957.
850 Arp, G., Hoffmann, V.-E., Seppelt, S., and Riegel, W.: Trias und Jura von Göttingen und
851 Umgebung, 74. Jahrestagung der Paläontologischen Gesellschaft, 2.-8.10.2004, Exkursion,
852 6, 147–192, Göttingen (Universitätsdrucke), 2004.

853 Arp, G., Bielert, F., Hoffmann, V.-E., and Löffler, T.: Palaeoenvironmental significance of
854 lacustrine stromatolites of the Arnstadt Formation ("Steinmergelkeuper", Upper Triassic,
855 N-Germany), Facies, 51, 419–441, 2005.
856 Baker, P.A. and Burns, S.J.: Occurrence and formation of dolomite in organic-rich continental
857 margin sediments, Am. Assoc. Petrol. Geol. Bull., 69, 1917–1930, 1985.
858 Balci, N., Menekşe, M., Karagüler, N.G., Sönmez, M.S., and Meister, P.: Reproducing
859 authigenic carbonate precipitation in the hypersaline Lake Acıgöl (Turkey) with microbial
860 cultures, Geomicrobiology Journal, 33, 758-773, 2016.
861 Bontognali, T.R.R., Vasconcelos, C., Warthmann, R.J., Bernasconi, S.M., Dupraz, C.,
862 Strohmenger, C.J., and McKenzie, J.A.: Dolomite formation within microbial mats in the
863 coastal sabkha of Abu Dhabi (United Arab Emirates), Sedimentology, 57, 824–844, 2010.
864 Bontognali T.R.R., McKenzie J.A., Warthmann R. and Vasconcelos C. (2013) Microbially
865 influenced formation of Mg-calcite and Ca-dolomite in the presence of exopolymeric
866 substances produced by sulphate-reducing bacteria. Terra Nova, 26, 72–77.
867 Bouton, A., Vennin, E., Pace, A., Bourillot, R., Dupraz, C., Thomazo, C., Brayard, A.,
868 Désaubliaux, G., and Visscher, P.T.: External controls on the distribution, fabrics and
869 mineralization of modern microbial mats in a coastal hypersaline lagoon, Cayo Coco
870 (Cuba), Sedimentology, 63, 972–1016, 2016.
871 Brack, P., Mundil, R., Oberli, F., Meier, M., and Rieber, H.: Biostratigraphic and radiometric
872 age data question the Milankovitch characteristics of the Latemar cycles (Southern Alps,
873 Italy), Geology, 24, 371–375, 1996.
874 Brack, P., Rieber, H., and Urlichs, M.: Pelagic successions in the Southern Alps and their
875 correlation with the Germanic Middle Triassic, Zentralbl. Geol. Paläontol. Teil I, 7–8,
876 853–876, 1999.

877 Breitenbach, S.F.M. and Bernasconi, S.M.: Carbon and oxygen isotope analysis of small
878 carbonate samples (20 to 100 μg) with a GasBench II preparation device, Rapid Commun.
879 Mass Spectrom., 25, 1910–1914, 2011.
880 Burns, S.J., McKenzie, J.A., and Vasconcelos, C.: Dolomite formation and biogeochemical
881 cycles in the Phanerozoic, Sedimentology, 47, 49–61, 2000.
882 Breda, A. and Preto, N.: Anatomy of an Upper Triassic continental to marginal-marine
883 system: the mixed siliciclastic–carbonate Travenanzes Formation (Dolomites, Northern
884 Italy), Sedimentology, 58, 1613-1647, 2011.
885 Chilingar, G.V.: Relationship between Ca/Mg ratio and geological age, AAPG Bull., 40,
886 2256–2266, 1956.
887 Clayton, R.N., Jones, B.F., and Berner, R.A.: Isotope studies of dolomite formation under
888 sedimentary conditions, Geochim. Cosmochim. Acta, 32, 415–432, 1968.
889 Cleveland, D.M., Nordt, L.C., and Atchley, S.C.: Paleosols, trace fossils, and precipitation
890 estimates of the uppermost Triassic strata in northern New Mexico. Palaeogeography,
891 Palaeoclimatology, Palaeoecology, 257, 421–444, 2008.
892 Court, W.M., Paul, A., and Lokier, S.W.: The preservation potential of environmentally
893 diagnostic sedimentary structures from a coastal sabkha, Marine Geology, 386, 1–18,
894 2017.
895 Czurda, K. and Nicklas, L.: Zur Mikrofazies und Mikrostratigraphie des Hauptdolomites und
896 des Plattenkalk-Niveaus der Klostertaler Alpen und des Rhätikon (Nördliche Kalkalpen,
897 Vorarlberg), In: Festband 300 Jahre Geol. Inst. Univ. Innsbruck, pp. 165–253, 1970.
898 Dal Corso, J., Mietto, P., Newton, R.J., Pancost, R.D., Preto, N., Roghi, G., and Wignall, P.B.
899 Discovery of a major negative $\delta^{13}C$ spike in the Carnian (Late Triassic) linked to the
900 eruption of Wrangellia flood basalts, Geology, 40, 79–82, 2012.
901 Deelman, J.C.: Low-temperature nucleation of magnesite and dolomite, Neues Jahrbuch für
902 Mineralogie (Stuttgart), Monatshefte, 7, 289–302, 1999.

903 Demicco, R.V. and Hardie, L.A.: Sedimentary structures and early diagenetic features of
904 shallow marine carbonate deposits, SEPM Atlas, Ser., 1, 265, 1994.
905 DePaolo, D.J. and Ingram, B.: High-resolution stratigraphy with strontium isotopes. Science,
906 227, 938–941, 1985.
907 De Zanche, V., Gianolla, P., Mietto, P., Siorpaes, C., and Vail, P.R.: Triassic sequence
908 stratigraphy in the Dolomites (Italy), Sci. Geol. Mem., 45, 1–27, 1993.
909 Doglioni, C.: Tectonics of the Dolomites (Southern Alps-Northern Italy), J. Structural
910 Geology, 9, 181–193, 1987.
911 Eugster, H.P. and Hardie, L.A.: Saline lakes, In: A. Lerman (Ed): Lakes, Chemistry, Geology,
912 Physics. Springer-Verlag, New York, N.Y., pp. 237-293, 1978.
913 Eugster, H.P. and Surdam, R.C.: Depositional environment of the Green River Formation of
914 Wyoming: a preliminary report, Bull. Geol. Soc. Am., 84, 1115-1120, 1973.
915 Fischer, A.G.: The Lofer cyclothems of the Alpine Triassic, Kansas Geol. Surv. Bull. 169,
916 107–149, 1964.
917 Flügel, E.: Microfacies of carbonate rocks - analysis, interpretation and application, 2nd.
918 Edition, Springer-Verlag Berlin Heidelberg, 2010.
919 Frisia, S.: Mechanisms of complete dolomitization in a carbonate shelf: comparison between
920 the Norian Dolomia Principale (Italy) and the Holocene of Abu Dhabi Sabkha, In: A
921 volume in honour of Dolomieu (Eds: B. Purser, M. Tucker, and D. Zenger), Spec. Publs.
922 Int. Ass. Sediment., 21, 55-74, 1994.
923 Frisia, S. and Wenk, H.-R.: TEM and AEM study of pervasive, multi-step dolomitization of
924 the upper Triassic Dolomia Principale (Northern Italy), J. Sed. Petrol., 63, 1049–1058,
925 1993.
926 Füchtbauer, H. and Goldschmidt, H.: Beziehungen zwischen Calzium-Gehalt und
927 Bildungsbedingungen der Dolomite, Geologische Rundschau, 55, 29–40, 1966.

928 Gattolin, G., Breda, A., and Preto, N.: Demise of Late Triassic carbonate platforms triggered
929 the onset of a tide-dominated depositional system in the Dolomites, Northern Italy,
930 Sedimentary Geology, 297, 38–49, 2013.
931 Gattolin, G., Preto, N., Breda, A., Franceschi, M., Isottona, M., and Gianolla P.: Sequence
932 stratigraphy after the demise of a high-relief carbonate platform (Carnian of the
933 Dolomites): Sea-level and climate disentangled, Palaeogeogr., Palaeoclimatol., Palaeoecol.
934 423, 1–17, 2015.
935 Garzanti, E., Gnaccolini, M., and Jadoul, F.: Anatomy of a semiarid coastal system: the Upper
936 Carnian of Lombardy (Italy), Riv. Ital. Paleontol. Stratigr., 101, 17–36, 1995.
937 Gianolla, P., De Zanche, V., and Mietto, P.: Triassic sequence stratigraphy in the Southern
938 Alps (Northern Italy): definition of sequences and basin evolution, In: Mesozoic and
939 Cenozoic Sequence Stratigraphy of European Basins (Eds. deGraciansky P.-C., J.
940 Hardenbol, T. Jacquin and P.R. Vail), SEPM Spec. Publ., 60, 719–747, 1998.
941 Ginsburg, R.N.: Landward movement of carbonate mud: new model for regressive cycles in
942 carbonates (abs.), AAPG Bull., 55, 340, 1971.
943 Given, R.K. and Wilkinson, B.H.: Dolomite abundance and stratigraphic age: constraints on
944 rates and mechanisms of Phanerozoic dolostone formation: perspectives, J. Sediment.
945 Research, 57, 1068–1078, 1987.
946 Gregg, J.M., Bish, D.L., Kaczmarek, S.E., and Machel, H.G.: Mineralogy, nucleation and
947 growth of dolomite in the laboratory and sedimentary environment: A review,
948 Sedimentology 62, 1749–1769, 2015.
949 Handy, M.R., Schmid, S.S., Bousquet, R., Kissling E., and Bernoulli, D.: Recoiling plate-
950 tectonic reconstructions of Alpine Tethys with the geological-geophysical record of
951 spreading and subduction in the Alps, Earth-Science Reviews 102, 121–158, 2010.
952 Hill, Jr., W.E., and Evans, D.R.: Solubility of twenty minerals in selected versene (EDTA)
953 solutions. State Geological Survey Kansas, Bull. 175, pp. 22, 1965.

954 Hsü, K.J. and Siegenthaler, C.: Preliminary experiments on hydrodynamic movement induced
955 by evaporation and their bearing on the dolomite problem, Sedimentology, 12, 11–25,
956 1969.
957 Hsü, K.J. and Schneider, J.: Progress report on dolomitization hydrology of Abu Dhabi
958 Sabkhas, Arabian Gulf, The Persian Gulf. Springer, New York, pp. 409–422, 1973.
959 Iannace, A. and Frisia, S.: Changing dolomitization styles from Norian to Rhaetian in
960 southern Tethys realm, In: A Volume in Honour of Dolomieu (Eds. B. Purser, M. Tucker
961 and D. Zenger), Int. Assoc. Sedimentol. Spec. Publ., 21, 75–89, 1994.
962 Illing, L.V., Wells, A.J. and Taylor, J.C.M.: Penecontemporary dolomite in the Persian Gulf,
963 In: Dolomitization and limestone diagenesis (Eds L.C. Pray and L.C. Murray), SEPM
964 Spec. Publ., 13, 89–111, 1965.
965 Jones, B.F.: The hydrology and mineralogy of Deep Springs Lake, Inyo County, California,
966 US Geol. Surv. Prof. Paper, 502-A, 56, 1965.
967 Korte, C., Kozur, H.W., Bruckschen, P., and Veizer, J.: Strontium isotope evolution of Late
968 Permian and Triassic seawater, Geochim. Cosmochim. Acta 67, 47–62, 2003.
969 Kraus, O.: Die Raibler Schichten des Drauzuges (Südliche Kalkalpen), Lithofazielle,
970 sedimentpetrographische und paläogeographische Untersuchungen. Jb. Geol. B.-A., 112,
971 81–152, 1969.
972 Land, L.S.: Failure to precipitate dolomite at 25°C from dilute solution despite 1000-fold
973 oversaturation after 32 years, Aquat. Geochem., 4, 361–368, 1998.
974 Last, W.M.: Lacustrine dolomite – an overview of modern, Holocene, and Pleistocene
975 occurrences, Earth-Science Reviews, 27, 221–263, 1990.
976 Liu, D., Xu, Y., Papineau, D., Yub, N., Fan, Q., Qiu, X., and Wang, H.: Experimental
977 evidence for abiotic formation of low-temperature proto-dolomite facilitated by clay
978 minerals, Geochim. Cosmochim. Acta, 247, 83–95, 2019.

979 Lumsden, D.N.: Discrepancy between thin-section and X-ray estimates of dolomite in
980 limestone, J. Sed. Petrol., 49, 429–435, 1979.
981 Machel, H.G.: Concepts and models of dolomitization: a critical reappraisal. Geological
982 Society, London, Special Publications, 235, 7–63, 2004.
983 Mather, C.C., Skrzypek, G., Dogramaci, S., and Grierson, P.F.: Paleoenvironmental and
984 paleohydrochemical conditions of dolomite formation within a saline wetland in arid
985 northwest Australia, Quaternary Science Reviews, 185, 172–188, 2018.
986 McArthur, J.M., Howarth, R.J., and Shield, G.A.: Strontium isotope stratigraphy. The
987 geologic time scale, 2012, In: Gradstein, F.M., Ogg, J.G., Schmotz, M.D. and Ogg, G.M.
988 (eds.), Elsevier, 1 of 2, 1144 pp, 2012.
989 McCormack, J., Bontognali, T.R.R., Immenhauser, A., and Kwiecien, O.: Controls on cyclic
990 formation of Quaternary early diagenetic dolomite, Geophysical Research Letters, 45,
991 3625–3634, 2018.
992 McKenzie, J.: Holocene dolomitzation of calcium carbonate sediments from the coastal
993 sabkhas of Abu Dhabi, U.A.E.. J. Geol., 89, 185–198, 1981.
994 McKenzie, J., Hsü, K.J., and Schneider, J.F.: Movement of subsurface waters under the
995 sabkha, Abu Dhabi, UAE and its relation to evaporative dolomite genesis. Spec. Publ.-
996 SEPM, 28, 11–30, 1980.
997 Meister, P., Bernasconi, S., McKenzie, J.A., Vasconcelos, C., Frank, M., Gutjahr, M., and
998 Schrag, D., Dolomite formation in the dynamic deep biosphere: Results from the Peru
999 Margin (ODP Leg 201), Sedimentology, 54, 1007–1032, 2007.
1000 Meister, P., Reyes, C., Beaumont, W., Rincon, M., Collins, L., Berelson, W., Stott, L.,
1001 Corsetti, F., and Nealson, K.H.: Calcium- and magnesium-limited dolomite precipitation at
1002 Deep Springs Lake, California, Sedimentology, 58, 1810–1830, 2011.
1003 Meister, P., McKenzie, J.A., Bernasconi, S.M., and Brack, P.: Dolomite formation in the
1004 shallow seas of the Alpine Triassic, Sedimentology, 60, 270–291, 2013.

1005 Meister, P., Frisia, S.: Dolomite formation by nano-crystal aggregation in the Dolomia
1006 Principale of the Brenta Dolomites (northern Italy). Rivista Italiana di Stratigrafia e
1007 Paleontologia, under revision.
1008 Missana, T., Garcia-Gutierrez, M., and Alonso, U.: Sorption of strontium onto illite/smectite
1009 mixed clays, Physics and Chemistry of the Earth, 33, 156–162, 2008.
1010 Moore, D.M. and Reynolds, R.C.: X-ray diffraction and the identification and analysis of clay
1011 minerals, Oxford University Press, New York, 378 p, 1997.
1012 Müller, D.W., Mueller, P.A., and McKenzie, J.A.: Strontium isotopic ratios as fluid tracers in
1013 Messinian evaporites of the Tyrrhenian Sea (western Mediterranean Sea), In: Kastens,
1014 K.A., Mascle, J., et al., Proc. ODP, Sci. Results, 107: College Station, TX (Ocean Drilling
1015 Program), 603–614, 1990a.
1016 Müller, D.W., McKenzie, J.A., and Mueller, P.A.: Abu Dhabi sabkha, Persian Gulf, revisited:
1017 application of strontium isotopes to test an early dolomitization model, Geology, 18, 618–
1018 621, 1990b.
1019 Muttoni, G., Kent, D.V., Garzanti, E., Brack, P., Abrahamsen, N., and Gaetani, M.: Early
1020 Permian Pangea 'B' to Late Permian Pangea 'A', Earth Planet. Sci. Lett., 215, 379–394,
1021 2003.
1022 Neri, C., Gianolla, P., Furlanis, S., Caputo, R., and Bosellini, A.: Note illustrative della Carta
1023 Geologica d'Italia alla scala 1:50.000, Foglio 029 Cortina d'Ampezzo, A.P.A.T. System
1024 Cart, Roma, 200 pp, 2007.
1025 Neuhuber, S., Steier, P., Gier, S., Draganits, E., and Kogelbauer, I.: Radiogenic Carbon
1026 Isotopes in Authigenic Carbonate from Lake Neusiedl, Austria, Geophysical Research
1027 Abstracts, 17, 15399–15399, 2015.
1028 Ogg, J.G.: Triassic, In: Gradstein, F. M., Ogg, J. G., Schmitz, M., and Ogg, G. (Eds.), The
1029 geologic time scale 2012, Elsevier, Cambridge University Press, Cambridge, 681–730,
1030 2012.

1031 Perri, E., Tucker, M.E., Słowakiewicz, M., Whitaker, F., Bowen, L., and Perrotta, I.D.:
1032 Carbonate and silicate biomineralization in a hypersaline microbial mat (Mesaieed sabkha,
1033 Qatar): Roles of bacteria, extracellular polymeric substances and viruses, Sedimentology,
1034 65, 1213–1245, 2018.
1035 Peterson, M.N.A., Bien, G.S., and Berner, R.A.: Radiocarbon studies of recent dolomite from
1036 Deep Springs Lake, California. J. Geophys. Res., 68, 6493–6505, 1963.
1037 Preto, N. and Hinnov, L.A.: Unravelling the origin of shallow-water cyclothems in the Upper
1038 Triassic Dürrenstein Formation (Dolomites, Italy). J. Sed. Res., 73, 774–789, 2003.
1039 Preto, N., Breda, A., Corso, J. D., Spötl, C., Zorzi, F., and Frisia, S.: Primary dolomite in the
1040 Late Triassic Travenanzes Formation, dolomites, Northern Italy: facies control and
1041 possible bacterial influence, Sedimentology, 62, 697–716, 2015.
1042 Randazzo, A.F. and Zachos, L.G.: Classification and description of dolomitic fabrics of rocks
1043 from the Floridan aquifer, U.S.A. Sediment. Geol., 37, 151–162, 1983.
1044 Ratschbacher, L., Merle, O., Davy, P., and Cobbold, P.: Lateral extrusion in the Eastern Alps,
1045 Part 1: Boundary conditions and experiments scaled for gravity, Tectonics, 10, 245–256,
1046 1991.
1047 Reinhardt, L. and Ricken, W.: The stratigraphic and geochemical record of Playa Cycles:
1048 monitoring a Pangaean monsoon-like system (Triassic, Middle Keuper, S. Germany),
1049 Palaeogeogr., Palaeoclimatol., Palaeoecol., 161, 205–227, 2000.
1050 Rodriguez-Blanco, J.D., Shaw, S., and Benning, L.G.: A route for the direct crystallization of
1051 dolomite, American Mineralogist, 100, 1172–1181, 2015.
1052 Rosen, M.R., Miser, D.E., Starcher, M.A., and Warren, J.K.: Formation of dolomite in the
1053 Coorong region, South Australia, Geochim. Cosmochim. Acta, 53, 661–669, 1989.
1054 Rosenbaum J. and Sheppard S.M.: An isotopic study of siderites, dolomites and ankerites at
1055 high temperatures, Geochim. Cosmochim. Acta 50, 1147–1150, 1986.

1056 Russo, F., Neri, C., Mastandrea, A., and Baracca, A.: The mud mound nature of the Cassian
1057 Platform Margins of the Dolomites A case history: the Cipit boulders from Punta
1058 Grohmann (Sasso Piatto Massif, northern Italy), Facies, 36, 25–36, 1997.
1059 Sánchez-Román, M., Vasconcelos, C., Warthmann, R., Rivadeneyra, M.A., and McKenzie,
1060 J.A.: Microbial dolomite precipitation under aerobic conditions: results from Brejo do
1061 Espinho Lagoon (Brazil) and culture experiments, Int. Assoc. Sediment. Spec. Publ., 40,
1062 167–178, 2009.
1063 Sánchez-Román, M., McKenzie, J.A., Rebello Wagener, A., Romanek, C.S., Sánchez-Navas,
1064 A., and Vasconcelos, C.: Experimentally determined biomediated Sr partition coefficient
1065 for dolomite: Significance and implication for natural dolomite, Geochim. Cosmochim.
1066 Ac., 75, 887–904, 2011.
1067 Seegis, D.: Die Lehrbergschichten im Mittleren Keuper von Süddeutschland: Stratigraphie,
1068 Petrographie, Paläontologie, Genese, Hennecke, Remshalden, 382 pp, 1997.
1069 Stampfli, G.M. and Borel, G.D.: A plate tectonic model for the Paleozoic and Mesozoic
1070 constrained by dynamic plate boundaries and restored synthetic oceanic isochrons, Earth
1071 Planet. Sci. Lett., 196, 17–33, 2002.
1072 Teal, C.S., Mazzullo, S.J., and Bischoff, W.D.: Dolomitization of Holocene shallow-marine
1073 deposits mediated by sulfate reduction and methanogenesis in normal-salinity seawater,
1074 northern Belize, J. Sediment. Research, 70, 649–663, 2000.
1075 Vahrenkamp, V.C. and Swart, P.K.: New distribution coefficient for the incorporation of
1076 strontium into dolomite and its implications for the formation of ancient dolomites,
1077 Geology, 18, 387–391, 1990.
1078 Van Tuyl, F.M.: The origin of dolomite, Annual Report 1914, Iowa Geological Survey, XXV,
1079 257–421, 1914.

1080 Vasconcelos, C., McKenzie, J.A., Warthmann, R., and Bernasconi, S.: Calibration of the $\delta^{18}O$
1081 paleo-thermometer with dolomite formed in microbial cultures and natural environments.
1082 Geology, 33, 317–320, 2005.
1083 Vasconcelos, C., Warthmann, R., McKenzie, J.A., Visscher, P.T., Bittermann, A.G., and van
1084 Lith, Y.: Lithifying microbial mats in Lagoa Vermelha, Brazil: Modern Precambrian
1085 relics? Sedimentary Geology, 185, 175–183, 2006.
1086 Veizer, J., Ala, D., Azmy, K., Bruckschen, P., Buhl, D., Bruhn, F., Carden, G.A.F., Diener,
1087 A., Ebneth, S., Godderis, Y., Jasper, T., Korte, C., Pawellek, F., Podlaha, O.G., and
1088 Strauss, H.: $^{87}Sr/^{86}Sr$, $\delta^{13}C$ and $\delta^{18}O$ evolution of Phanerozoic seawater, Chemical geology,
1089 161, 59–88, 1999.
1090 Von der Borch, C.C.: Stratigraphy and formation of Holocene dolomitic carbonate deposits of
1091 the Coorong area, South Australia, J. Sediment. Research, 46, 952–966, 1976.
1092 Von der Borch, C.C., Lock, D.E., and Schwebel, D.: Ground-water formation of dolomite in
1093 the Coorong region of South Australia, Geology, 3, 283–285, 1975.
1094 Warren, J.: Sedimentology and mineralogy of dolomitic Coorong Lakes, South Australia, J.
1095 Sedimentary Petrol., 60, 843–858, 1990.
1096 Warren, J.: Dolomite: occurrence, evolution and economically important associations, Earth-
1097 Science Reviews, 52, 1–81, 2000.
1098 Wenk, H.R., Meisheng, H., and Frisia, S.: Partially disordered dolomite: microstructural
1099 characterization of Abu Dhabi sabkha carbonates, Am. Mineral., 78, 769–774, 1993.
1100

1101 **Figure Captions**

1102 **Figure 1.** (**a**) Palaeogeographic map of ~~the~~ Southern Alpine to Germanic domains during the
1103 middle Triassic, reproduced from Brack et al. (1999; modified). Bal: Balaton; BG: Burgundy
1104 Gate; Car: Carnian Alps; ECG: eastern Carpathian Gate; Lomb: Lombardy; NCA: Northern
1105 Calcareous Alps; SMG: Silesian Moravian Gate. Inset: Tectonic map of the Southern Alps

(Brack et al., 1996, modified) showing the sampling location at Rifugio Dibona. GL: Giudicarie Line; PL: Pustertal Line; VL: Val Sugana Line. (**b**) Stratigraphy of the middle to late Triassic in Venetian Alps, showing a transition in geometries from basin and platform topotraphy during the Lower Carnian to an extended alluvial to tidal plain in this Upper Carnian. The shaded area indicates the Travenanzes Fm., showing a lateral transition in facies and a transgressive boundary to the Dolomia Principale. Compiled from Breda and Preto (2011), after De Zanche et al. (1993), modified.

Figure 2. Stratigraphic section at Rifugio Dibona: (**a**) Complete section modified after Breda and Preto (2011); (**a**) detailed section of uppermost part of the clay-rich interval, showing sampling locations. (**c**) Outcrop photograph showing the uppermost grey part of the clay-rich interval with the location of the profile shown in (b).

Figure 3. Outcrop images of different types of dolomite intercalated in red and grey clay of the Travenanzes Fm. at Rifugio Dibona: (**a**) Homogeneous dolomite bed (15 cm thick; 33 m). (**b**) Upper part: dolomite nodules embedded in red clay, crosscut by green coloured cracks as part of a calcic vertisol (95 m). (**c**) Laminated dolomite (110-112 m) in grey clay. (**d**) Bed with gypsum nodules, and cracks filled with gypsum, at 50 m; (**e**) Dolomite-cemented conglomerate bed at 75 m. (**f**) Laminated bed showing soft sediment deformation (106 m); an isoclinal synsedimentary fold is indicated by the arrow. (**g**) Laminated dolomite showing folding of the laminae due to soft sediment deformation (same bed as in f).

Figure 4. Photomicrographs of thin sections of dolomites of the Travenanzes Fm.: (**a**) Rounded mud clasts embedded in dolomicrite matrix. The larger mm-size intraclast in the upper left side of the image (arrow) consists itself of matrix with darker embedded mudclasts (sample TZ16-St1; 104 m). (**b**) Mud clasts in dolomicrite matrix. Mudclasts are deformed and

layers of coarser and finer matrix are equally affected by plastic deformation (sample TZ16-22; 120 m). (**c**, **d**) Pseudomorphs after gypsum in fine-grained dolomudstone (arrows). (**e**) Oolitic grainstone (sample TZ14-4; 64 m). The cortices consist of microcrystalline dolomite lacking a radial structure. Some show a concentric structure (arrow). (**f**) Laminated dolomite showing pseudo-teepee structures (arrow). Vertical cracks are often, but not always, associated with pseudo-teepees (sample TZ14-10; 107 m). Some coarser grained laminae may contain microsparite and peloids (P). (**g**) Laminated dolomite showing both plastic and brittle deformation of laminae. A cm-scale pseudo-teepee occurs in the centre of the image (sample TZ 16-21; 107 m). (**h**, **i**) Closeup of graded lamina in (g) showing plastic deformation. The top of the lamina shows an erosion surface with small rip-up clasts (arrow), overlain by a coarser layer.

Figure 5. SEM images of dolomites in backscatter mode: (**a**) Overview showing layer enriched in celestine inclusions (bright areas) in dolomite (Sample TZ14-9d; 95 m); (**b**) Celestine inclusion with barite in the centre (same sample as in a); (**c**) Barite crystals in dolomicrite (sample TZ14-4; 65 m).

Figure 6. SEM images of dolomites in backscatter mode showing different types of crystal shape: (**a**) Spheroidal growth of dolomite (darker areas) in clay layers (brighter areas; sample TZ14-9d; 95 m). (**b**) Closeup of a. (**c**) Dolomite crystals showing a porous interior domain but homogeneous syntaxial cement rims (sample TZ14-12; 90 m). (**d**) Similar as in (c; sample TZ14-9d; 95 m).

Figure 7. X-ray diffraction patterns: (**a**) Bulk analyses of homogeneous dolomite (Samples TZ14-1, TZ14-7, and TZ14-9); main peaks and ordering peaks are labelled with (hkl) indices. (**b**-**d**) Clay mineral separates of samples TZ14-1, TZ14-7 and TZ14-9, air dried (N), saturated

with ethylene glycol (EG), and heated to 550°C (T); d-values in Å. In the ethylene-glycol saturated sample TZ14-9 ~~the illite-smectite mixed-layer is best seen~~. The arrow points ~~at~~ the expandable (smectite) part of the mixed-layer.

Figure 8. (**a**) Carbon/oxygen isotope cross-plot. (**b**) Oxygen isotope values through the stratigraphic section.

Figure 9. Element concentrations in sequentially extracted fractions of bulk dolomite and clay samples of the Travenanzes Fm.: (**a**) Ca vs. Mg; (**b**) Sr vs. K.

Figure 10. Comparison of Sr-isotopes in dolomites of the Travenanzes Fm. with Carnian seawater curve (Korte et al., 2003). The 2-sigma uncertainties are smaller than the symbol size.

Figure 11. Sr-isotope values ~~from~~ dolomites ~~of~~ different modern and ancient environments: Travenanzes Fm. ~~in~~ the Dolomites, Southern Alps; Germanic Keuper (Weser Formation and Arnstadt Formation); Coorong Lagoon; Deep Springs Lake. $^{87}Sr/^{86}Sr$ ratios of modern seawater are from DePaolo and Ingram (1985).

TABLES

Table 1. ~~Compilation of~~ sedimentary structures from thin section analysis of dolomites from the Travenanzes Fm. at the Dibona section.

Table 2. Relative abundances and ordering parameters of dolomites from the Travenanzes Formation. Relative abundances were estimated based on the 104 peak height. The stoichiometry Mg/(Ca+Mg) was determined from the shift of the 104 peak using the equation

of Lumsden (1979). The structural ordering was calculated from the ratio of the 015 ordering peak to the 110 peak according to Füchtbauer and Goldschmidt (1966).

Table 3. Total inorganic and organic carbon (TIC, TOC) contents of clay samples from the Travenanzes Formation.

Table 4. Carbon and oxygen isotope values of different types of dolomite from the Travenanzes Formation.

Table 5. Element concentrations of leacheates from dolomites and clays used for Sr-isotope analysis.

Table 6. Compiled $^{87}Sr/^{86}Sr$ ratios of sequentially leached dolomites from different locations, clays and test minerals using different extraction solutions.

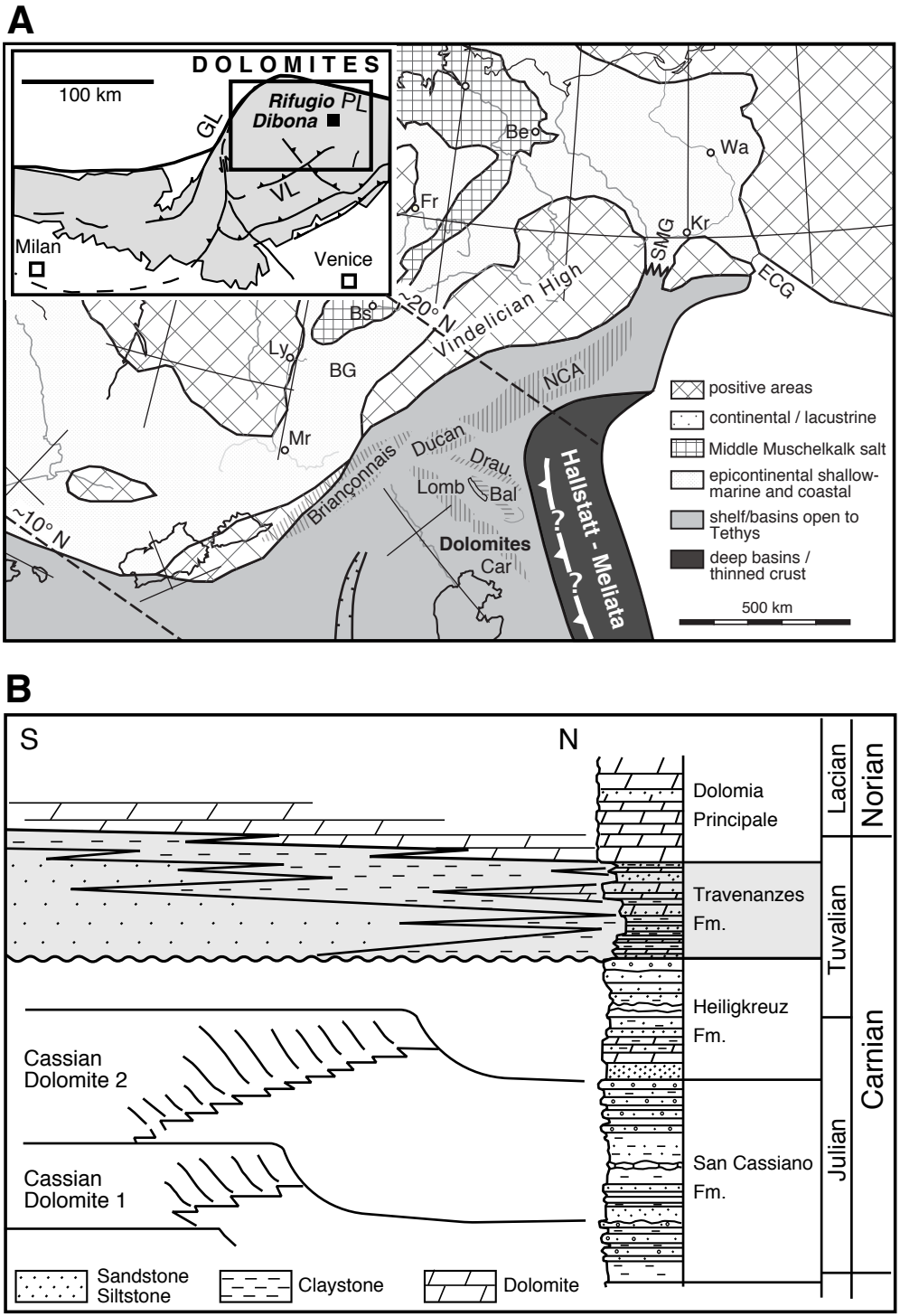
A
DOLOMITES
100 km
Rifugio PL
Dibona
GL
VL
Milan
Venice
Be
Wa
Fr
Kr
SMG
ECG
Bs
Ly
BG
Vindelician High
NCA
Mr
Briançonnais
Ducan
Drau
Lomb
Bal
Dolomites
Car
Hallstatt - Meliata
~20° N
~10° N
positive areas
continental / lacustrine
Middle Muschelkalk salt
epicontinental shallow-marine and coastal
shelf/basins open to Tethys
deep basins / thinned crust
500 km
B
S
N
Dolomia Principale
Travenanzes Fm.
Heiligkreuz Fm.
San Cassiano Fm.
Cassian Dolomite 2
Cassian Dolomite 1
Lacian
Norian
Tuvalian
Julian
Carnian
Sandstone Siltstone
Claystone
Dolomite

Figure 1

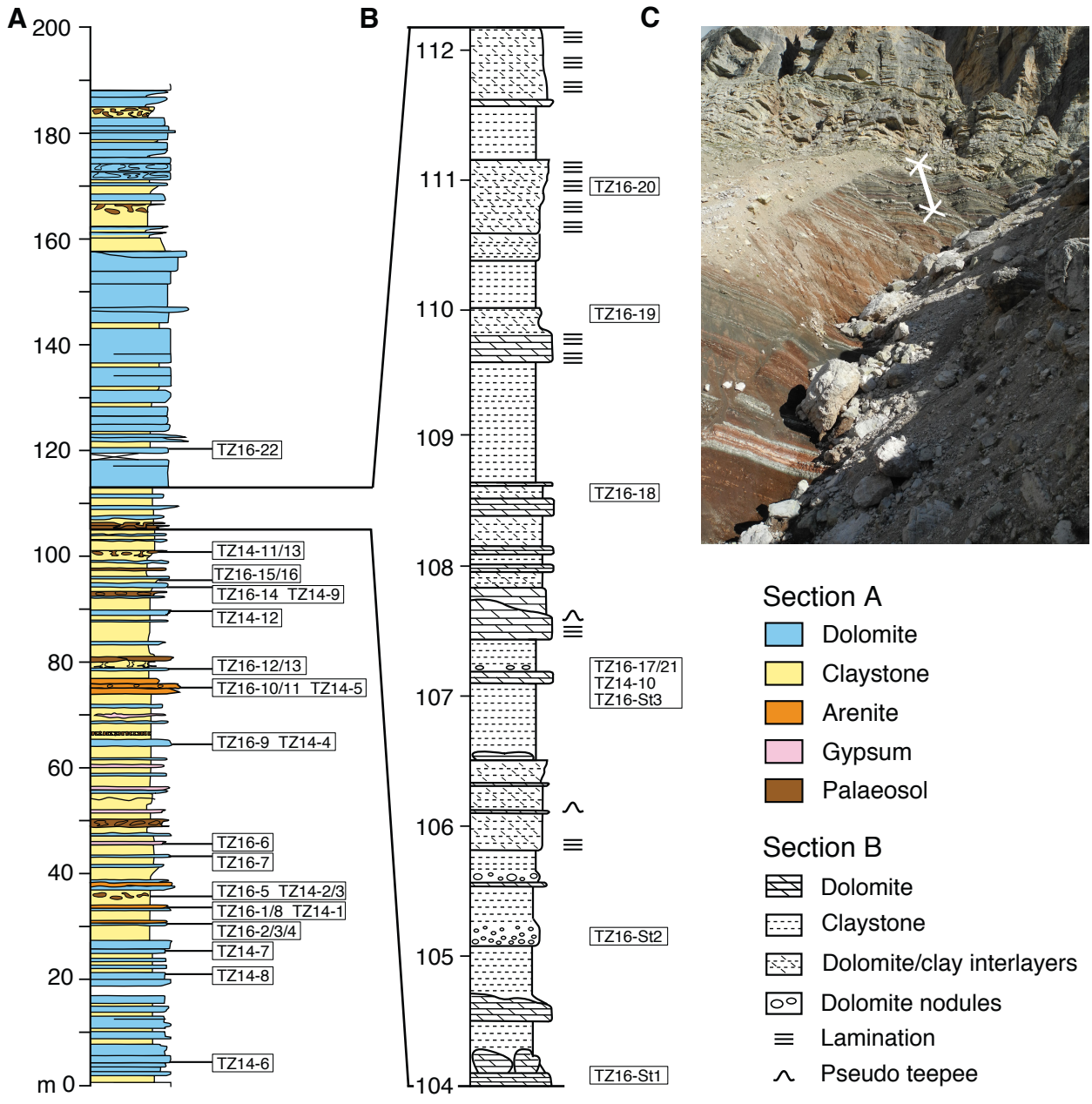
A
B
C
200
180
160
140
120
100
80
60
40
20
m 0
112
111
110
109
108
107
106
105
104
TZ16-22
TZ14-11/13
TZ16-15/16
TZ16-14 TZ14-9
TZ14-12
TZ16-12/13
TZ16-10/11 TZ14-5
TZ16-9 TZ14-4
TZ16-6
TZ16-7
TZ16-5 TZ14-2/3
TZ16-1/8 TZ14-1
TZ16-2/3/4
TZ14-7
TZ14-8
TZ14-6
TZ16-20
TZ16-19
TZ16-18
TZ16-17/21
TZ14-10
TZ16-St3
TZ16-St2
TZ16-St1
Section A
Dolomite
Claystone
Arenite
Gypsum
Palaeosol
Section B
Dolomite
Claystone
Dolomite/clay interlayers
Dolomite nodules
Lamination
Pseudo teepee

Figure 2

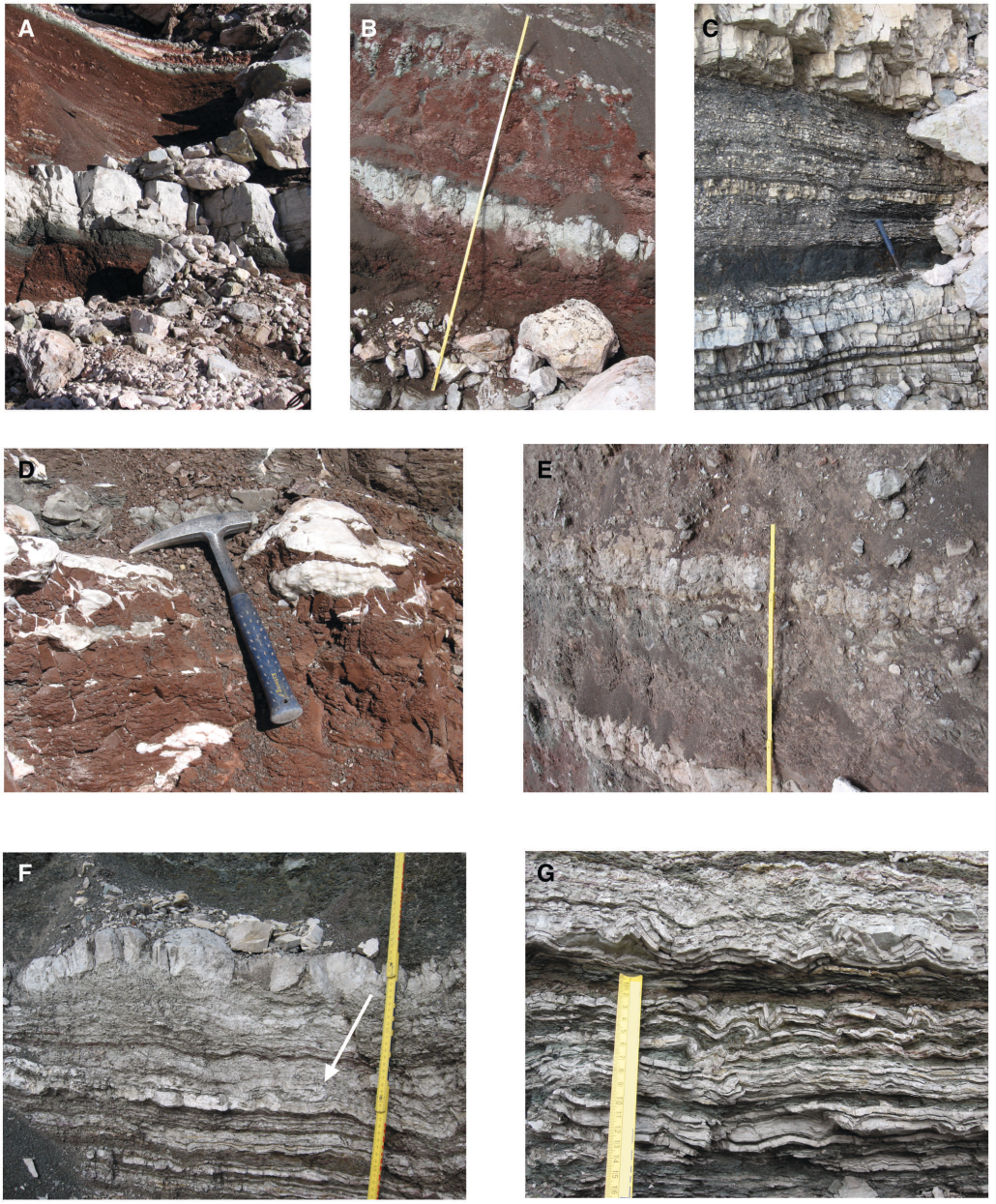

Figure 3

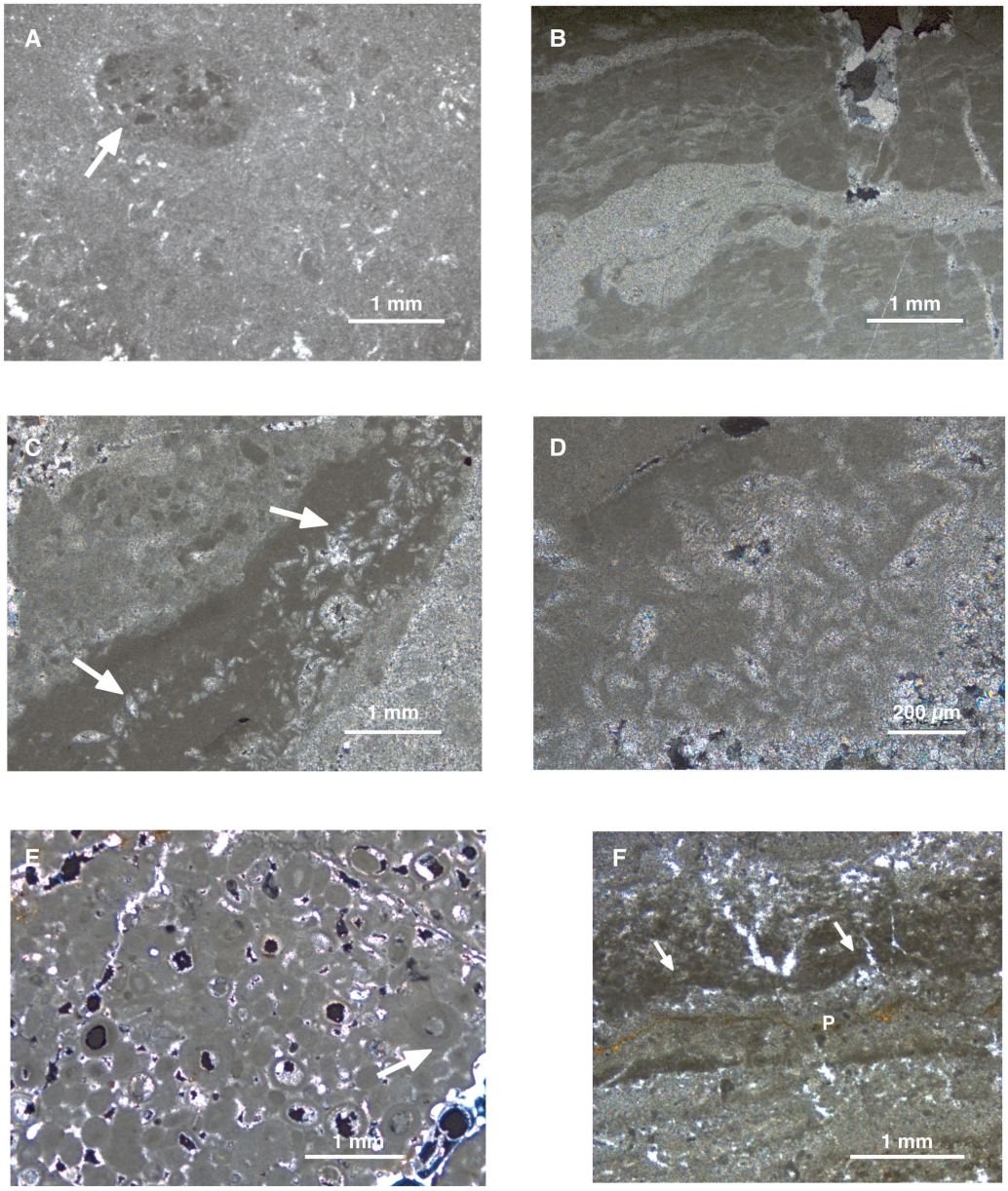

Figure 4

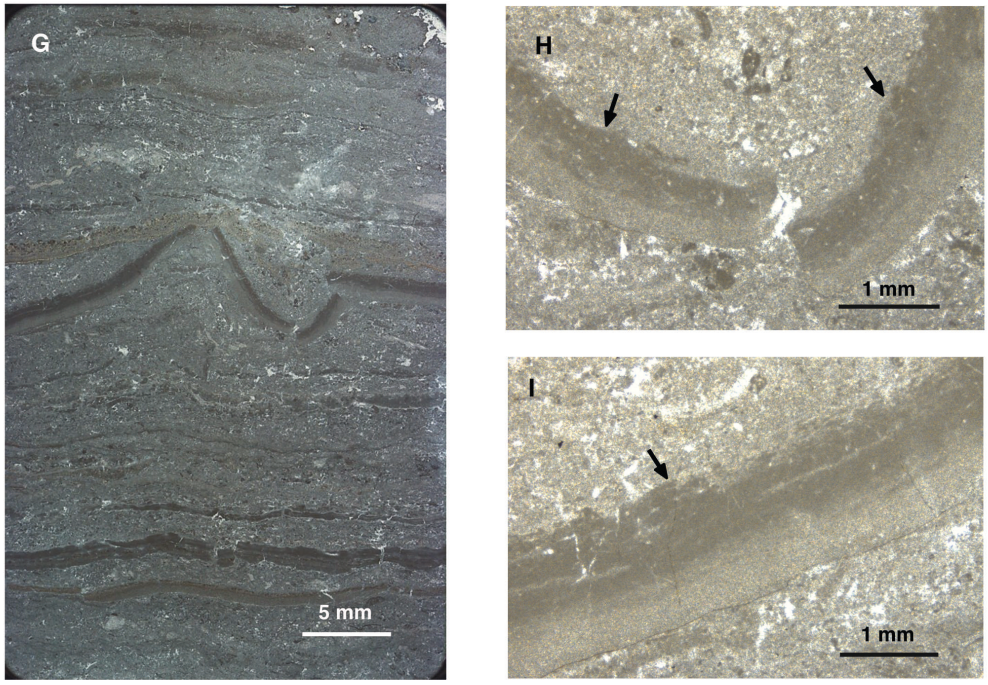

Figure 4 continued

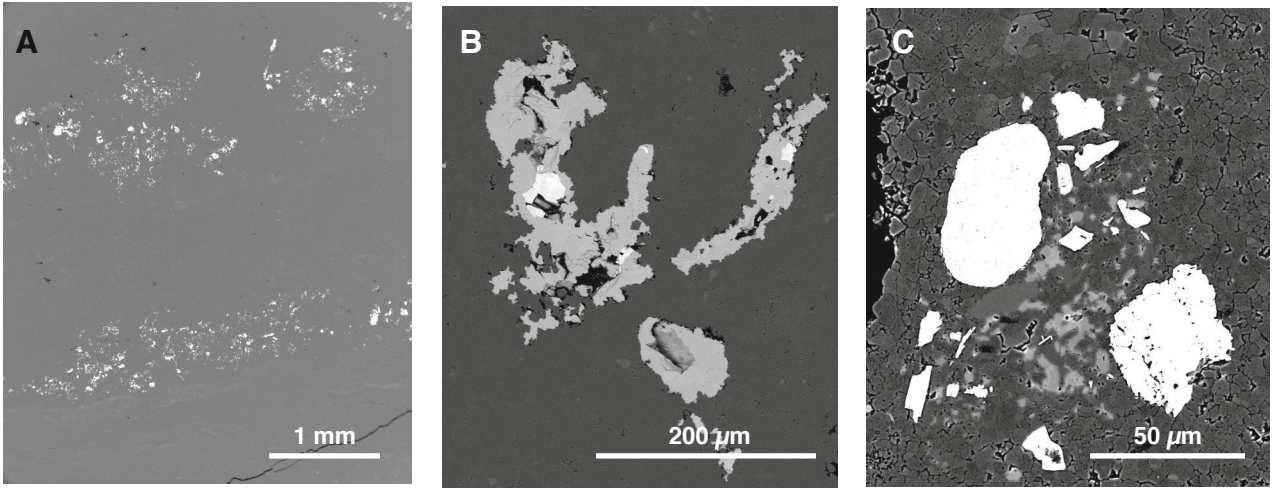

Figure 5

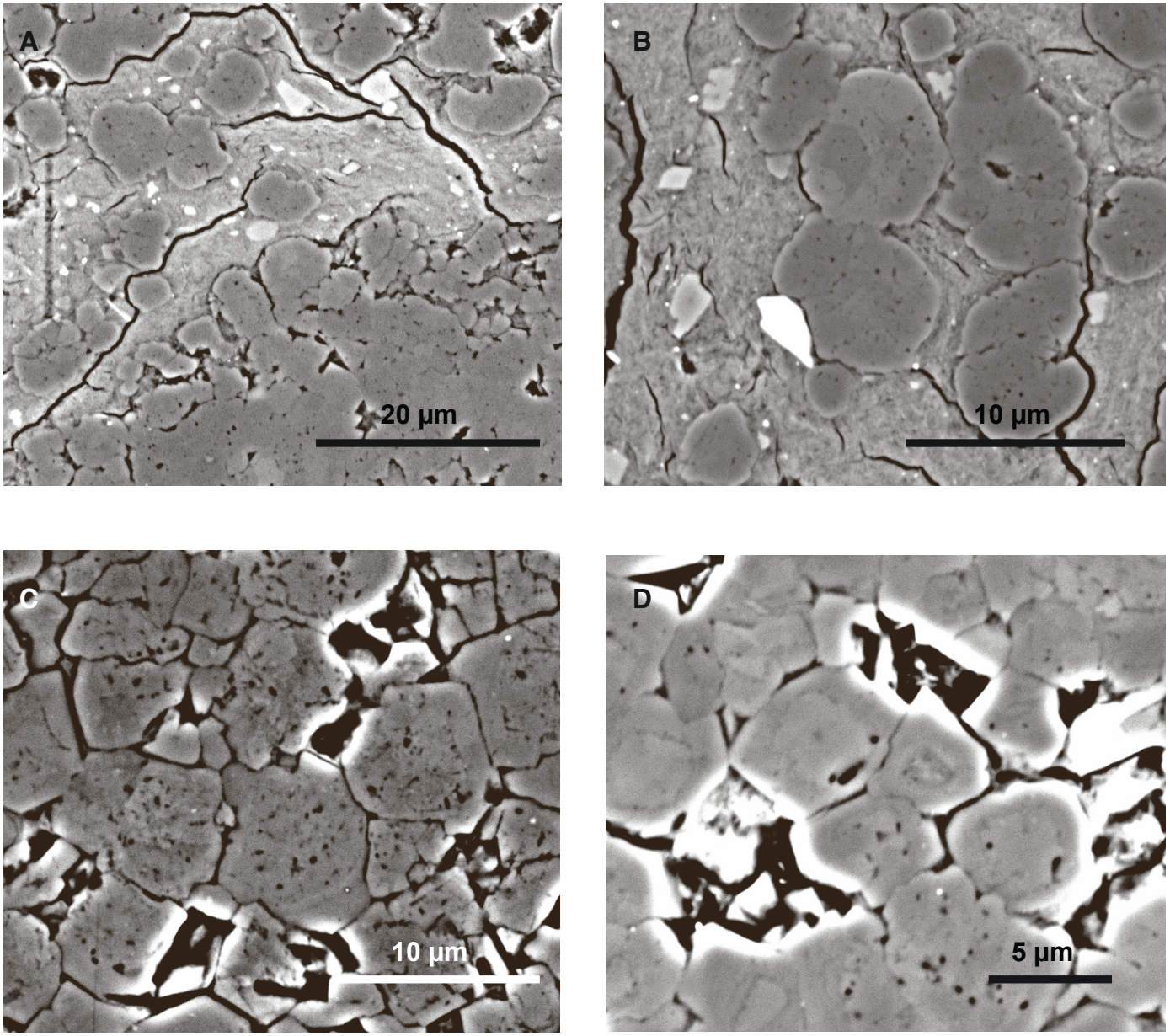

Figure 6

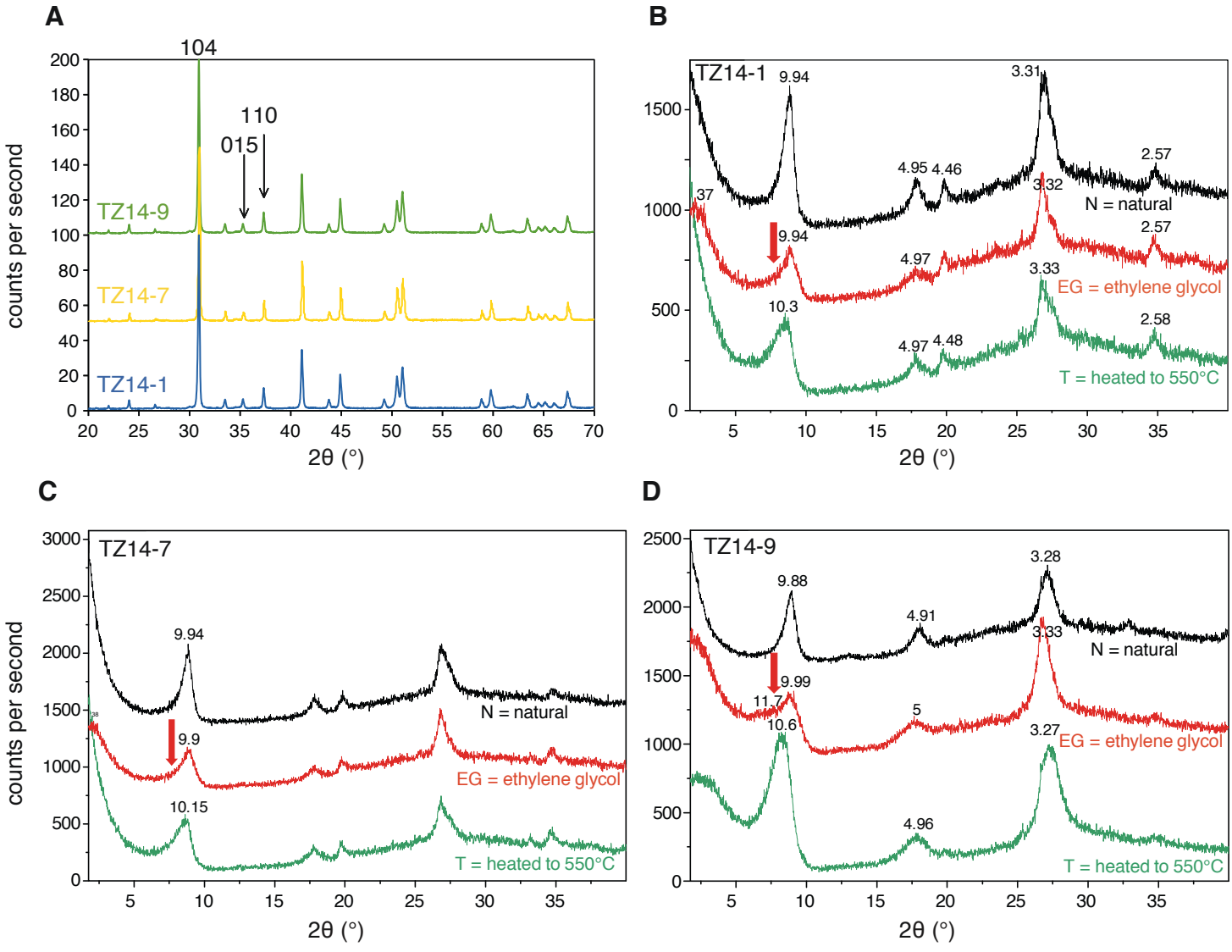
A
104
110
015
TZ14-9
TZ14-7
TZ14-1
counts per second
2θ (°)
B
TZ14-1
9.94
3.31
4.95
4.46
2.57
3.32
N = natural
37
9.94
2.57
4.97
3.33
EG = ethylene glycol
10.3
2.58
4.97
4.48
T = heated to 550°C
2θ (°)
C
TZ14-7
9.94
N = natural
9.9
EG = ethylene glycol
10.15
T = heated to 550°C
counts per second
2θ (°)
D
TZ14-9
9.88
3.28
4.91
3.33
N = natural
9.99
11.7
10.6
5
3.27
EG = ethylene glycol
4.96
T = heated to 550°C
2θ (°)

Figure 7

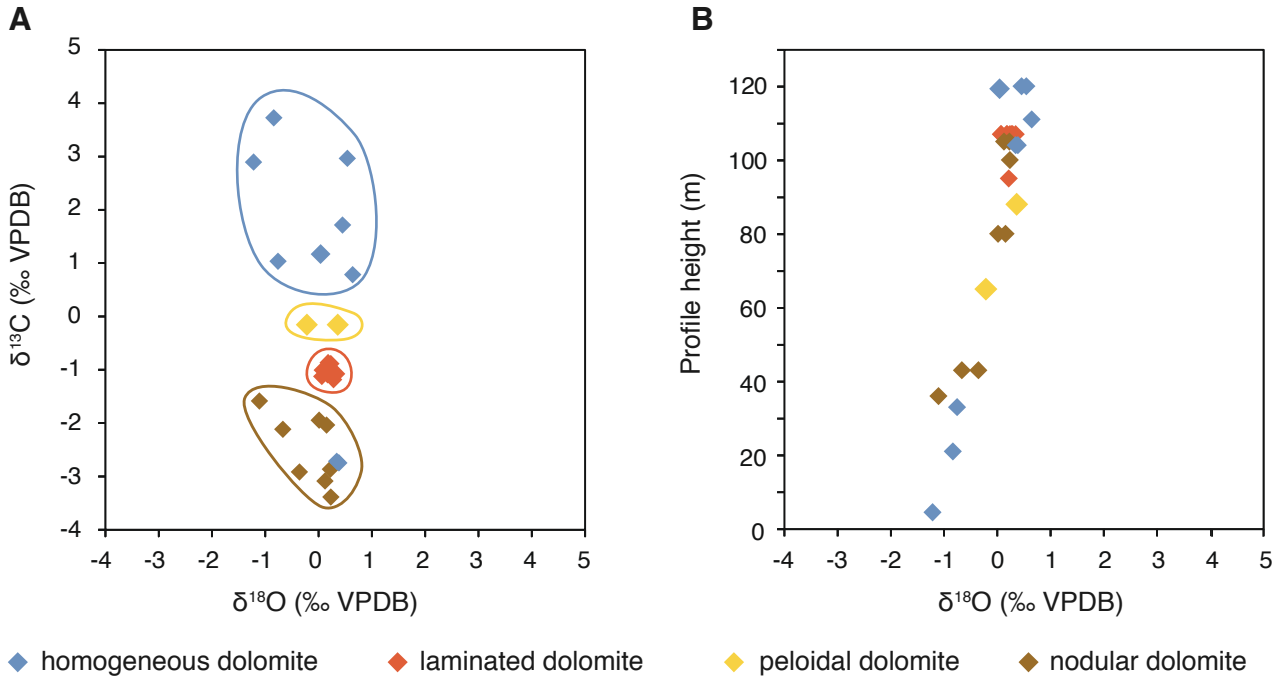
A
B
δ13C (‰ VPDB)
δ18O (‰ VPDB)
Profile height (m)
δ18O (‰ VPDB)
homogeneous dolomite
laminated dolomite
peloidal dolomite
nodular dolomite

Figure 8

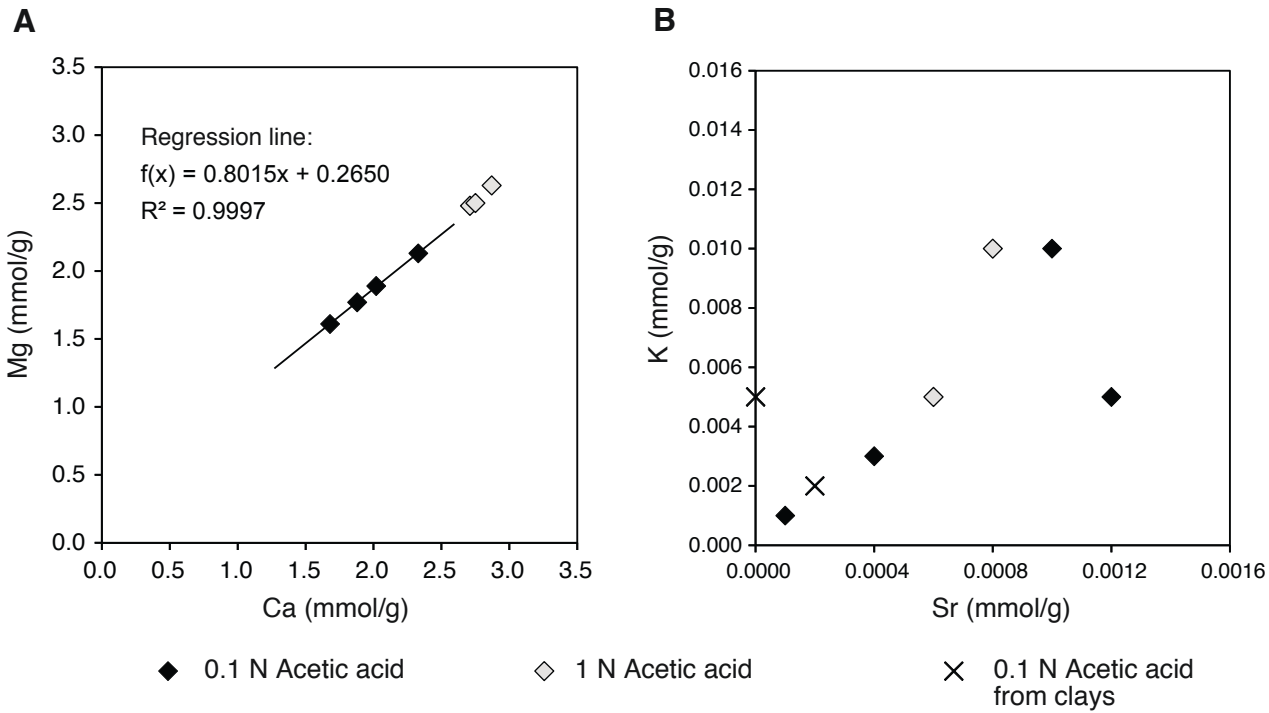
A
B
Regression line:
f(x) = 0.8015x + 0.2650
R² = 0.9997
Mg (mmol/g)
Ca (mmol/g)
K (mmol/g)
Sr (mmol/g)
0.1 N Acetic acid
1 N Acetic acid
0.1 N Acetic acid from clays

Figure 9

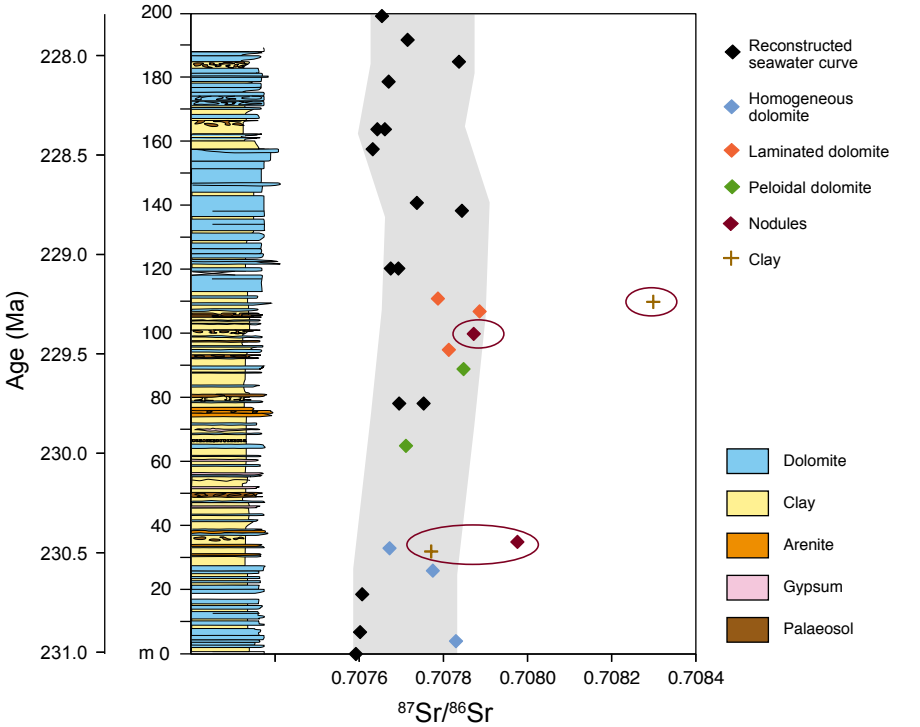
Age (Ma)
228.0
228.5
229.0
229.5
230.0
230.5
231.0
200
180
160
140
120
100
80
60
40
20
m 0
0.7076
0.7078
0.7080
0.7082
0.7084
87Sr/86Sr
Reconstructed seawater curve
Homogeneous dolomite
Laminated dolomite
Peloidal dolomite
Nodules
Clay
Dolomite
Clay
Arenite
Gypsum
Palaeosol

Figure 10

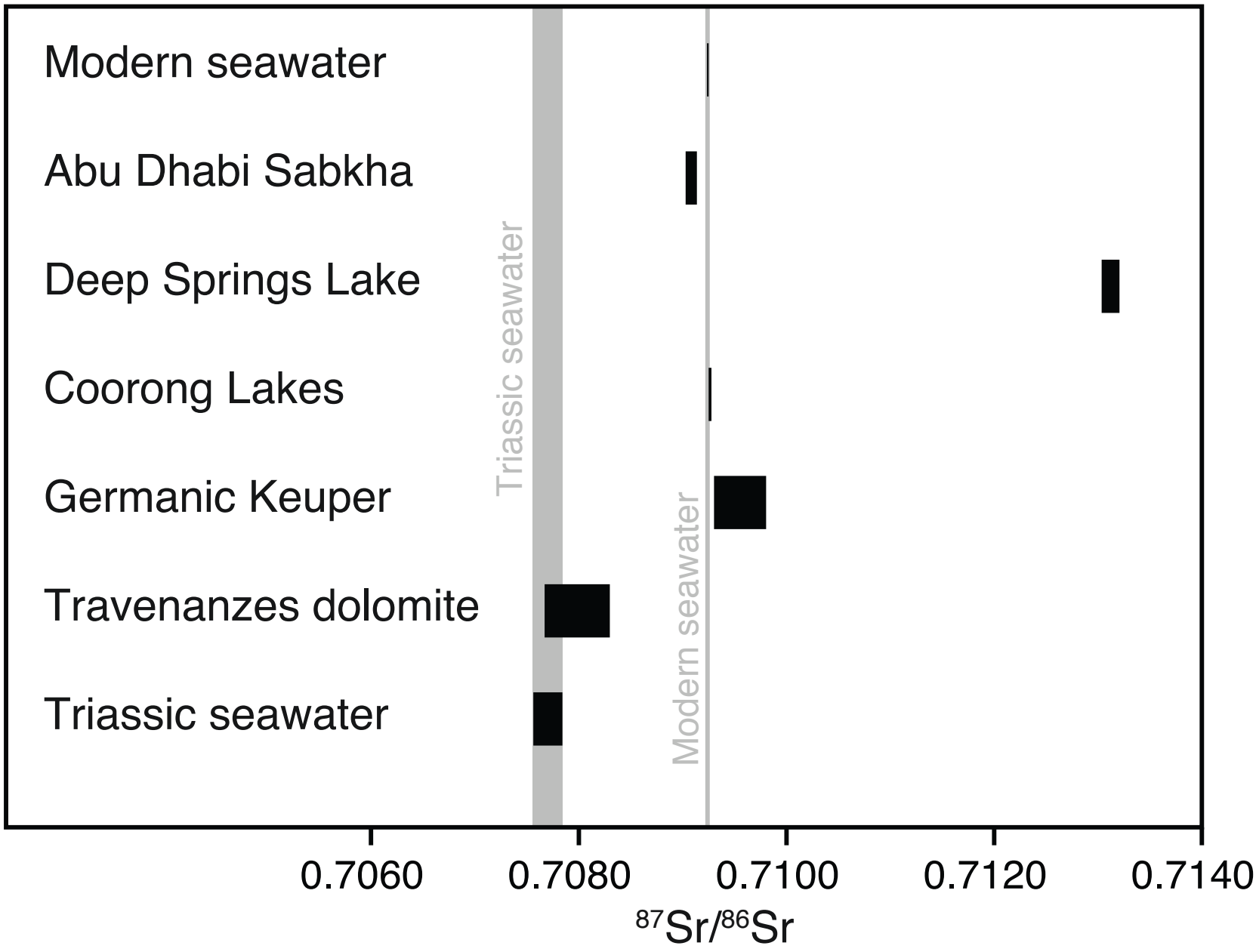
Modern seawater
Abu Dhabi Sabkha
Deep Springs Lake
Coorong Lakes
Germanic Keuper
Travenanzes dolomite
Triassic seawater
Triassic seawater
Modern seawater
0.7060
0.7080
0.7100
0.7120
0.7140
87Sr/86Sr

Figure 11

Table 1

Macroscopic Description	Height	Samples		Matrix			Allochems							Sedimentary structures				Porosity		Deformation		SMF**
		2014	2016	Aphano-topic	Micro-spar	Cavity-filling cement	Undeform. mud clasts*	Deformed mud clasts	Flat pebbles	Packed peloids	Ooids	Quartz clasts	Bioclasts	Lamination	Graded Bedding	Pseudo-Teepee	Erosion surfaces	Fenestral Porosity	Moldic porosity	Soft sediment deformation	Brittle deformation	
dolomite with pyrite	120.0		TZ16-22	+	+	+	++	+	-	+	-	-		+	-	-	+	+	+	+	++	25
laminated dolomite/clay	111.0	TZ14-11	TZ16-20	++	+	+	+	±	+	±	-	-		++	+	+	±	-	-	+	++	25
laminated dolomite	107.0	TZ14-10	TZ16-21/St-3	+	+	+	+	±	-	+	-	-		++	+	+	++	+	-	+	+	25
laminite	107.0		TZ16-17	++	+	-	+	+	+	-	-	-	+	±	±	-	-	+	++	+	+	25
dolomite nodule	105.0		TZ16-St-2	++	+	-	+	+	±	-	-	-		-	-	-	-	-	-	+	+	diag.
homogeneous dolomite	104.0		TZ16-St-1	++	+	±	+	±	-	±	-	-		-	-	-	-	-	-	+	+	23
nodular dolomite	100.0	TZ14-13		++	+	-	+	±	-	-	-	-		-	-	-	-	-	-	±	+	diag.
dolomite nodule	96.0		TZ16-15	++	±	+	++	±	±	±	-	-		-	-	-	-	-	-	++	++	diag.
laminated dolomite	95.0	TZ14-9		+	-	+	+	+	±	±	-	-		++	+	+	+	+	-	+	+	25
porous dolomite	89.0	TZ14-12		+	±	-	+	±	-	-	-	-	Forams Biocl.	-	-	-	-	+	++	+	+	23
nodular bed	80.0		TZ16-13	++	+	+	+	±	-	-	-	-	(+)	-	-	-	-	±	+	+	-	diag.
palaeosol, nodule	79.0		TZ16-12	+	±	±	+	±	-	-	-	-		-	-	-	-	-	+	++	++	diag.
sandy dolomite (congl.)	75.0	TZ14-5	TZ16-11	++	±	±	++	±	++	-	-	+	Ostracods (+)	-	-	-	-	±	±	-	-	23
sandstone	74.0		TZ16-10	+	±	-	++	-	-	-	-	+		-	-	-	-	-	-	-	-	25
brittle porous dolomite	65.0	TZ14-4		+	-	+	±	-	-	±	+	-	Forams +	(-)	+	-	-	+	+	+	+	15
porous dolomite	43.0		TZ16-7	++	±	+	±	±	-	-	-	-	Ostracods ±	-	-	-	-	±	+	++	+	23
nodules of dolomite	35.0	TZ14-3		++	+	-	-	±	-	-	-	-		-	-	-	-	-	-	+	+	diag.
dolomite nodule	35.0	TZ14-2		+	±	-	-	±	-	-	-	-		-	-	-	-	-	-	+	+	diag.
arenite	33.5		TZ16-8	+	±	-	+	-	-	++	-	++		-	+	-	-	-	-	+	+	Sst.
homogeneous dolomite	33.0	TZ14-1		++	±	-	±	+	-	±	-	±		±	±	-	-	-	-	+	+	23
laminated dolomite	31.5		TZ16-2	+	-	-	+	-	-	-	-	++		+	+	-	+	+	-	±	±	Sst.
palaeosol, dolomit	30.1		TZ16-3	++	-	±	+	±	-	-	-	-		-	-	-	-	-	-	+	+	diag.
red mottled dolomite	26.0	TZ14-7		-	-	-	±	±	-	-	-	-		-	-	-	±	-	-	±	±	23
dolomite with clay	21.0	TZ14-8		++	±	-	±	±	-	-	-	-		±	-	-	-	-	-	-	-	23
homogeneous dolomite	4.0	TZ14-6		++	+	±	+	±	-	±	-	-	Forams +	+	+	+	+	-	+	+	±	25

- not present ± rare + common ++ very abundant (+) putative

** Nodules are most likely diagenetic and can thus not be associated to a microfacies

* Needs to be further subdivided into peloids, intraclasts, flat pebbles and clast of brittle deformation

Homogeneous dolomite | Laminated dolomite | Nodular dolomite | Oolithic dolomite | Sandstone

Table 2

Sample	Depth (m)	d(A°)	Ca/(Ca+Mg) (%)	015/110
TZ14-1	33.0	2.88944	51.1	0.44
TZ14-7	43.0	2.88871	50.9	0.41
TZ14-9	95.0	2.88633	50.1	0.46

Table 3

Sample	TC (wt%)	TOC (wt%)	TIC (wt%)
TZ16-1	0.06	0.05	0.02
TZ16-19B	0.12	0.11	0.02
TZ16-5	0.16	0.05	0.12
TZ16-19A	0.34	0.10	0.25
TZ16-14	0.42	0.16	0.27
TZ16-18	0.50	0.07	0.43
TZ16-16	0.51	0.05	0.46

Table 4

Sample	Depth (m)	$\delta^{13}C$ (‰ VPDB)	$\delta^{18}O$ (‰ VPDB)	Type	Description
TZ14-1	33	1.04	-0.76	homogeneous	with siliciclastis
TZ14-3	35	-1.58	-1.11	nodule	with barite
TZ14-4	65	-0.15	-0.22	peloidal	with apatite
TZ14-6	4	2.90	-1.22	homogeneous	with siderite and pyrite
TZ14-8	21	3.73	-0.84	homogeneous	with clay, apatite and Fe-oxide
TZ14-9	95	-1.01	0.21	laminated	with celestine and barite
TZ14-10b	107	-1.05	0.26	laminated	with apatite and pyrite
TZ14-11	111	0.79	0.64	homogeneous	homog. Lamina with clay and pyrite
TZ14-12	89	-0.15	0.36	peloidal	with megalodont and Ti-oxides
TZ14-13	100	-3.38	0.23	nodule	palaeosol with Fe-oxide
TZ16-St1	104	-2.74	0.38	homogeneous	mud clast top
	104	-2.71	0.34	homogeneous	matrix
TZ16-St2	105	-3.08	0.12	nodule	matrix top
	105	-2.86	0.22	nodule	matrix bottom
TZ16-7	43	-2.91	-0.36	*Rauhwacke*	matrix top
	43	-2.11	-0.67	*Rauhwacke*	matrix bottom
TZ16-13	80	-2.03	0.15	nodule	matrix top
	80	-1.94	0.01	nodule	matrix bottom
TZ16-21	107	-0.86	0.18	laminated	graded lamina
	107	-1.09	0.17	laminated	ligh lamina
	107	-0.88	0.23	laminated	dark lamina
TZ16-22	120	1.72	0.45	homogeneous	mud clast
	120	1.22	0.15	homogeneous	lamination
	120	2.97	0.54	homogeneous	homogeneous part
TZ16-St3	107	-1.07	0.34	laminated	dark layer, lense
	107	-1.00	0.07	laminated	dark layer bottom
	107	-1.18	0.28	laminated	dark layer top
	107	-1.12	0.06	laminated	light layer top

Table 5

Sample	Element	0.1 N acetic acid fraction				1 N acetic acid fraction			1 N HCl fraction	
		µmol/g	µmol/g	µmol/g	µmol/g	µmol/g	µmol/g	µmol/g	µmol/g	µmol/g
Bulk dolomite samples										
		TZ14-1	TZ14-7	TZ14-9	crystal	TZ14-1	TZ14-7	TZ14-9		
		0.098 g	0.127 g	0.099 g	0.094 g	0.098 g	0.127 g	0.099 g		
	Al	6.58	3.17	11.57	3.04	4.51	8.17	5.97		
	Ca (mmol/g)	1.68	2.33	1.88	2.50	2.87	2.71	2.75		
	Fe	4.97	3.53	10.67	34.27	2.04	9.15	5.02		
	K	3.32	9.71	5.26	0.93	10.31	4.65	13.51		
	Mg (mmol/g)	1.61	2.13	1.77	2.34	2.64	2.48	2.50		
	Mn	5.96	3.57	7.68	15.24	10.84	3.72	10.67		
	Na	12.78	18.98	17.32	1.85	17.35	20.12	23.30		
	P	1.50	n.d.	0.98	n.d.	0.20	1.45	n.d.		
	Ti	n.d.	n.d.	n.d.	n.d.	n.d.	n.d.	n.d.		
	Ba	0.50	0.03	0.48	n.d.	1.75	0.02	1.03		
	Sr	0.38	1.00	1.16	0.13	0.79	0.57	34.91		
	Rb	n.d.	n.d.	n.d.	n.d.	n.d.	n.d.	n.d.		
Clay samples										
		TZ16-1	TZ16-19B			TZ16-1	TZ16-19B		TZ16-1	TZ16-19B
		0.038 g	0.030 g			0.038 g	0.030 g		0.038 g	0.030 g
	Al	2.18	4.52			1.54	4.01		39.86	33.62
	Ca	19.14	11.62			8.48	4.34		0.71	0.60
	Fe	0.72	1.79			0.83	2.25		75.59	11.56
	K	4.97	9.02			2.77	3.69		11.69	12.61
	Mg	8.05	13.76			4.46	6.07		24.62	18.75
	Mn	n.d.	n.d.			n.d.	n.d.		n.d.	n.d.
	Na	0.355	0.470			0.305	0.389		0.531	0.828
	P	6.89	1.08			0.67	n.d.		n.d.	n.d.
	Ti	n.d.	n.d.			n.d.	n.d.		1.305	0.194
	Ba	n.d.	n.d.			n.d.	n.d.		0.022	n.d.
	Sr	0.417	0.047			0.187	0.018		0.017	0.005
	Rb	n.d.	n.d.			n.d.	n.d.		n.d.	n.d.

Table 6. Sr-isotopes

Sample	Section (m)	Description	Seq. extr.	Weight (mg)	Reagent	Amount (ml)	Extr. T (°C)	Extr. time	Shaker y/n	Washing (before step)	Run no.	$^{87}Sr/^{86}Sr$	2σ (10^{-6})	Aliquot for conc.
NBS987		Standard solution (500 ppm)		500 ng							(n = 40)	0.710272	4	
NBS988		Standard solution (500 ppm)		500 ng							(n = 9)	0.710268	6	
Test minerals														
Series 1 (sequential extraction)														
Celestine				2.34	1M NaCl	2 ml	20	12 h	n	1M NaCl	6052	0.708037	5	
Barite				25.09	0.1N AcOH	2 ml	20	12 h	n	3M NaCl, 1M KCl, H_2O, 0.1N AcOH	6109	0.708887	9	
Dolomite				9.88	0.1N AcOH	2 ml	20	12 h	n	3M NaCl, 1M KCl, H_2O, 0.1N AcOH	6110	0.709942	11	
Mixture		Barite 4.5 mg; Celestine 8.91 mg; Dolomite 35.9 mg	seq.	49.31	1M NaCl	2 ml	20	12 h	n	1M NaCl	6053	0.708038	3	
Mixture			seq.	-	0.1N AcOH	2 ml	20	12 h	n	3M NaCl, 1M KCl, H_2O, 0.1N AcOH	6108	0.709501	40	
Series 2														
Celestine				2.22	1M NaCl	2 ml	20	2 h	n	-	6121	0.708045	4	
Celestine				4.60	0.1N AcOH	2 ml	20	4 h	n	12h 1M NaCl	6132	0.708047	3	
Barite				36.94	6N HCl	2 ml	40	12 h	n	-	6152	0.707610	5	
Barite			seq	-	6N HCl	2 ml	40	12 h	n	-	6155	0.707564	6	
Dolomite				17.37	0.1N AcOH	5 ml	40	12 h	n	-	6068	0.710831	7	
Dolomite		Replicate		3.41	0.1N AcOH	2 ml	40	12 h	n	-	6114	0.710557	11	
Travenanzes Fm.														
Bulk samples sequential extractions, Series 1														
TZ14-1	33 m	homogeneous dolomite	seq.	12.35	1M NaCl	2 ml	20	12 h	n	-	6112	0.708125	12	
TZ14-1	33 m	homogeneous dolomite	seq.	-	0.1N AcOH	3 × 2 ml	20	4h, 12h, 4h	y	1M NaCl, H_2O, 3.3M KCl, H_2O	6169	0.707666	4	
TZ14-1	33 m	homogeneous dolomite	seq.	-	0.1N AcOH	2 ml	20	36 h	y	-	6173	0.715417	250	
TZ14-9	95 m	laminated dolomite	seq.	13.50	1M NaCl	2 ml	20	12 h	n	-	6113	0.707880	4	
TZ14-9	95 m	laminated dolomite	seq.	-	0.1N AcOH	3 × 2 ml	20	4h, 12h, 4h	y	1M NaCl, H_2O, 3.3M KCl, H_2O	6171	0.707817	5	
TZ14-9	95 m	laminated dolomite	seq.	-	0.1N AcOH	2 ml	20	36 h	y	-	6174	0.719226	455	
Mixture		Residue from test mineral series 1	seq.	-	0.1N AcOH	3 × 2 ml	20	4h, 12h, 4h	y	1M NaCl, H_2O, 3.3M KCl, H_2O	6172	0.709812	5	
Mixture		Residue from test mineral series 1	seq.	-	0.1N AcOH	2 ml	20	36 h	y	-	6176	0.709900	4	
TZ14-1	33 m	homogeneous dolomite		42.76	0.1N AcOH	2 ml	20	4 h	n	-	6130	0.707894	4	
TZ14-9	95 m	laminated dolomite		17.69	0.1N AcOH	2 ml	20	4 h	n	-	6131	0.707872	5	
Bulk samples sequential extractions, Series 2														
TZ14-1	33 m	homogeneous dolomite		93.91	1M NaCl	10 ml	20	12 h	y	-	6182	0.708096	5	
TZ14-1	33 m	homogeneous dolomite	seq.	98.28	0.1N AcOH	10 ml	20	12 h	y	-	6183	0.707812	4	yes
TZ14-1	33 m	homogeneous dolomite	seq.	-	1N AcOH	10 ml	20	12 h	y	-	6205	0.707670	5	yes
TZ14-1	33 m	homogeneous dolomite		50.00	6N HCl	5 ml	20	12 h	n	10h 1N CH_3COOH	6445	0.710403	6	
TZ14-7	26 m	mottled dolomite		90.64	1M NaCl	10 ml	20	12 h	y	-	6179	0.707883	4	
TZ14-7	26 m	mottled dolomite	seq.	127.52	0.1N AcOH	10 ml	20	12 h	y	-	6178	0.707801	4	yes
TZ14-7	26 m	mottled dolomite	seq.	-	1N AcOH	10 ml	20	12 h	y	-	6207	0.707719	4	yes
TZ14-7	26 m	mottled dolomite		50.00	6N HCl	5 ml	20	12 h	n	10h 1N CH_3COOH	6449	0.730453	5	
TZ14-9	95 m	laminated dolomite		97.82	1M NaCl	10 ml	20	12 h	y	-	6187	0.707869	3	
TZ14-9	95 m	laminated dolomite	seq.	98.76	0.1N AcOH	10 ml	20	12 h	y	-	6185	0.707862	3	yes
TZ14-9	95 m	laminated dolomite	seq.	-	1N AcOH	10 ml	20	12 h	y	-	6206	0.707813	3	yes
TZ14-9	95 m	laminated dolomite		50.00	6N HCl	5 ml	20	12 h	n	10h 1N CH_3COOH	6447	0.708464	4	
Dolomite (single crystal)		control		116.65	1M NaCl	10 ml	20	12 h	y	-	6184	0.708401	40	
Dolomite (single crystal)		control	seq.	94.12	0.1N AcOH	10 ml	20	12 h	y	-	6180	0.707735	6	yes
Dolomite (single crystal)		control	seq.	-	1N AcOH	10 ml	20	12 h	y	-	6208	0.707666	6	yes
Micro-drill samples														
TZ14-3	35 m	dolomite nodule		-	0.1N AcOH	2 ml	20	24 h	n	H_2O, 5min 0.1N AcOH	6548	0.707976	4	
TZ14-4	65 m	peloidal dolomite		-	0.1N AcOH	2 ml	20	24 h	n	H_2O, 5min 0.1N AcOH	6549	0.707711	4	
TZ14-6	4 m	homogeneous dolomite		-	0.1N AcOH	2 ml	20	24 h	n	H_2O, 5min 0.1N AcOH	6550	0.707830	4	
TZ14-8	21 m	dolomite with clay		-	0.1N AcOH	2 ml	20	24 h	n	H_2O, 5min 0.1N AcOH	6551	0.707821	4	
TZ14-10b	107 m	laminated dolomite		-	0.1N AcOH	2 ml	20	24 h	n	H_2O, 5min 0.1N AcOH	6554	0.707886	4	
TZ14-11	111 m	laminated dolomite		-	0.1N AcOH	2 ml	20	24 h	n	H_2O, 5min 0.1N AcOH	6553	0.707787	4	
TZ14-12	89 m	peloidal dolomite		-	0.1N AcOH	2 ml	20	24 h	n	H_2O, 5min 0.1N AcOH	6555	0.707848	4	
TZ14-13	100 m	dolomite with palaeosol		-	0.1N AcOH	2 ml	20	24 h	n	H_2O, 5min 0.1N AcOH	6556	0.707872	4	
Micro-drilled sequential extractions														
TZ14-1	33 m	homogeneous dolomite	seq.	-	0.1N AcOH	2 ml	20	24 h	n	H_20, 5min 0.1N AcOH	6411	0.707672	3	
TZ14-1	33 m	homogeneous dolomite	seq.	-	1N AcOH		20	24 h	n	H_20, 5min 0.1N AcOH	6448	0.708300	23	
TZ14-7	26 m	mottled dolomite	seq.	-	0.1N AcOH	2 ml	20	24 h	n	H_20, 5min 0.1N AcOH	6479	0.707775	6	
TZ14-7	26 m	mottled dolomite	seq.	-	1N AcOH		20	24 h	n	H_20, 5min 0.1N AcOH	6444	0.708502	22	
TZ14-7	26 m	clay layer	seq.	-	0.1N AcOH		20	24 h	n	H_20, 5min 0.1N AcOH	6410	0.707742	4	
TZ14-7	26 m	clay layer	seq.	-	1N AcOH		20	24 h	n	H_20, 5min 0.1N AcOH	6446	0.708467	2	
TZ14-9	95 m	laminated dolomite	seq.	-	0.1N AcOH	2 ml	20	24 h	n	H_20, 5min 0.1N AcOH	6412	0.707813	149	
TZ14-9	95 m	laminated dolomite	seq.	-	1N AcOH		20	24 h	n	H_20, 5min 0.1N AcOH	6443	0.708281	56	
Clay samples														
TZ16-1	32 m	red (green) clay	seq.	38.30	0.1N AcOH	2 ml	20	12 h	n	2h 0.1N AcOH	6557	0.707771	4	yes
TZ16-1	32 m	red (green) clay	seq.	-	1N AcOH	2 ml	20	12 h	n	2h 1N AcOH	6558	0.707768	4	yes
TZ16-1	32 m	red (green) clay	seq.	-	6N HCl	2 ml	20	12 h	n	4h 6N HCl	6559	0.722998	18	yes
TZ16-19B	110 m	dark grey clay	seq.	29.74	0.1N AcOH	2 ml	20	12 h	n	2h 0.1N AcOH	6560	0.708299	8	yes
TZ16-19B	110 m	dark grey clay	seq.	-	1N AcOH	2 ml	20	12 h	n	2h 1N AcOH	6561	0.708582	8	yes
TZ16-19B	110 m	dark grey clay	seq.	-	6N HCl	2 ml	20	12 h	n	4h 6N HCl	6552	0.733910	24	yes
Germanic Keuper														
Lehr		micro-drilled		-	0.1N AcOH	2 ml	20	24 h	n	H_20, 5min 0.1N AcOH	6545	0.709303	4	
Keu 1-2 B		micro-drilled		-	0.1N AcOH	2 ml	20	24 h	n	H_20, 5min 0.1N AcOH	6546	0.709805	6	
Deep Springs Lake														
DS11-3, 16.5	16.5 cm	dried mud	seq.	91.17	0.1N AcOH	10 ml	20	5 min	n	H_2O	6363	0.713207	4	
DS11-3, 16.5	16.5 cm	dried mud	seq.	-	0.1N AcOH	10 ml	20	10 h	n	H_2O	6363	0.713086	4	
DS11-3, 52.5	52.5 cm	dried mud		62.19	0.1N AcOH	10 ml	20	10 h	n	H_2O	6343	0.713035	4	
Milne Lake (Coorong)														
CM01-3	30 cm	dried mud, ground	seq.	47.94	0.1N AcOH	10 ml	20	5 min	n	H_2O	6340	0.709251	4	
CM01-3	30 cm	dried mud, ground	seq.	-	0.1N AcOH	10 ml	20	10 h	n	H_2O	6340	0.709275	3	
CM01-9	90 cm	dried mud, ground		52.47	0.1N AcOH	10 ml	20	10 h	n	H_2O	6341	0.709272	4	